# DLR-IB-RM-OP-2021-238

## Development and Actuation of a New Type of Gearbox for Mobile Robotics

**Studienarbeit**

Julia Richter

Deutsches Zentrum
DLR für Luft- und Raumfahrt

TECHNISCHE UNIVERSITÄT DRESDEN

IFA LS-AT

**Fakultät Elektrotechnik und Informationstechnik** Institut für Automatisierungstechnik

# Studienarbeit

zum Thema

## Development and Actuation of a New Type of Gearbox for Mobile Robotics

vorgelegt von Julia Richter
im Studiengang Mechatronik, Jg. 2017
geboren am 28.05.1998 in Erfurt

Betreuer: M. Sc. Alexander Kirst
Dipl.-Ing. Jens Reinecke
Verantwortlicher Hochschullehrer: Prof. Dr. techn. Klaus Janschek
Tag der Einreichung: 31.08.2021

TECHNISCHE UNIVERSITÄT DRESDEN

IFA LS-AT

Fakultät Elektrotechnik und Informationstechnik ● Institut für Automatisierungstechnik

# AUFGABENSTELLUNG FÜR DIE STUDIENARBEIT

Für: Frau Julia Richter, Matrikelnr.: 4691793
Studiengang: Mechatronik
Thema: **Entwicklung und Aktuierung eines neuartigen Schaltgetriebes für die mobile Robotik**

Das DLR (Deutsches Zentrum für Luft- und Raumfahrt) entwickelt im Zuge der Grundlagenforschung schaltbare Getriebe für die Robotik, die es ermöglichen bei wechselnden Aufgaben verschiedene Drehmomente und Drehzahlen zu erreichen. Beispiele für Anwendungen sind das Knie eines humanoiden Roboters oder die Radeinheit eines Rovers, bei denen ein Wechsel zwischen kraftvollen und dynamischen Bewegungen stattfindet.
Ein schon bestehendes Konzept für ein Schaltgetriebe mit zwei Gängen, soll im Rahmen dieser Semesterarbeit optimiert und weiterentwickelt werden. Der Fokus liegt dabei auf der Entwicklung und Integration der Aktuierung des Schaltens in das Gesamtsystem.
Die Festlegung auf eine Anwendung in der Lauf- oder Radrobotik erfolgt selbstständig. Unter Nutzung eines Modells können die Anforderungen abgeleitet und eine mögliche Ansteuerung erarbeitet werden. Nach einer Variantendiskussion soll ein entsprechender Schaltmechanismus entwickelt werden. Optional kann die Steuerung am Versuchsstand getestet werden, wenn die Fertigung und Inbetriebnahme rechtzeitig abgeschlossen sind.

Aufgaben:

- Strukturierte Anforderungsdefinition
- Analyse des bestehenden Konzeptes
- Simulation des Getriebeverhaltens mit Schaltaktuierung in Simulink
- Entwicklung einer Aktuierung für den Schaltvorgang sowie Konstruktion einer integrierten Baugruppe (bestehend aus Getriebe und Schaltung)
- Optional: Übertragung der Ansteuerung auf den Versuchsstand (wird im Rahmen der Anforderungsdefinition bestimmt)
- Verifikation der Anforderungen
- Dokumentation der Ergebnisse

Die verwendeten Ergebnisse anderer Arbeiten müssen im schriftlichen Teil eindeutig und vollständig gekennzeichnet und durch geeignete Zitierung belegt werden.
Es gelten die Richtlinien für wissenschaftliche und studentische Arbeiten des Instituts.
Die Studienarbeit wird in englischer Sprache verfasst.

Betreuer: Prof. Dr. techn. K. Janschek,
Betriebsbetreuer: M. Sc. A. Kirst, Dipl.-Ing J. Reinecke (DLR Wessling)

Ausgehändigt: 01.05.2021 Einzureichen: 31.08.2021

Klaus Janschek Digital unterschrieben von Klaus Janschek Datum: 2021.04.25 21:40:06 +02'00'

Prof. Dr. techn. K. Janschek
Verantwortlicher Hochschullehrer

Julia Richter Digital unterschrieben von Julia Richter Datum: 2021.04.26 16:10:49 +02'00'

Julia Richter
Studentin

TECHNISCHE UNIVERSITÄT DRESDEN

IFA LS-AT

**Fakultät Elektrotechnik und Informationstechnik** Institut für Automatisierungstechnik

# Entwicklung und Aktuierung eines neuartigen Schaltgetriebes für die mobile Robotik

Getriebe aller Art sind eine der Säulen der Mechanik. Speziell die Robotik stellt immer wieder neue Anforderungen an ihre Bauteile, weshalb permanent neue Getriebe entwickelt werden. Die Grundlage dieser Arbeit ist ein bereits bestehendes Konzept für ein neuartiges Schaltgetriebe, welches speziell für die Anwendung in der Robotik ausgelegt ist.

Der Fokus dieser Arbeit liegt auf der Schaltaktuierung dieses Getriebes. Zu Beginn werden verschiedene Aktuierungsmöglichkeiten diskutiert. Um die Dynamik zu verstehen, wird eine Simulation des Schaltverhaltens entwickelt. Neben der Umgebung Simulink wird dabei zusätzlich mit der Erweiterung Simscape sowie der Bibliothek Simscape Driveline gearbeitet. Mit Hilfe der Simulation werden die verschiedenen Antriebsvarianten geprüft und als Ergebnis ein konkretes Design empfohlen.

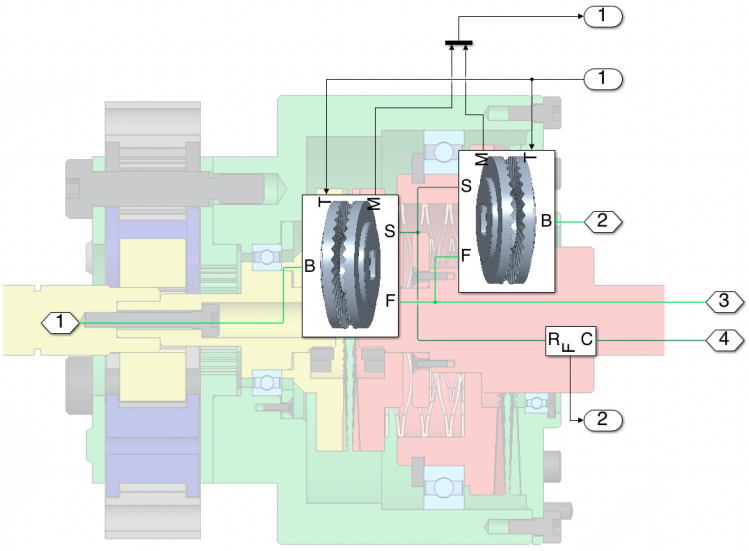


| | |
|---|---|
| Betreuer: | M. Sc. Alexander Kirst |
| | Dipl.-Ing. Jens Reinecke |
| Hochschullehrer: | Prof. Dr. techn. Klaus Janschek |
| Tag der Einreichung: | 31.08.2021 |

STUDIENARBEIT

Bearbeiter: Julia Richter

TECHNISCHE UNIVERSITÄT DRESDEN

IFA LS-AT

**Fakultät Elektrotechnik und Informationstechnik** Institut für Automatisierungstechnik

# Development and Actuation of a New Type of Gearbox for Mobile Robotics

Gearboxes of all kinds are one of the foundations of mechanics. Robotics in particular constantly places new demands on its components, which is why new gearboxes are constantly being developed. The foundation of this work is an already existing concept for a new switch-able gear, which is designed especially for applications in robotics.

The focus of this work is the actuation of this gearbox. At the beginning, different actuation possibilities are discussed. In order to understand the dynamics, a simulation of the shifting behaviour is developed. In addition to the Simulink environment, the extension Simscape and the Simscape Driveline library are used. The simulation is then applied to test the different actuation variants and as a result, a specific design will be recommended.

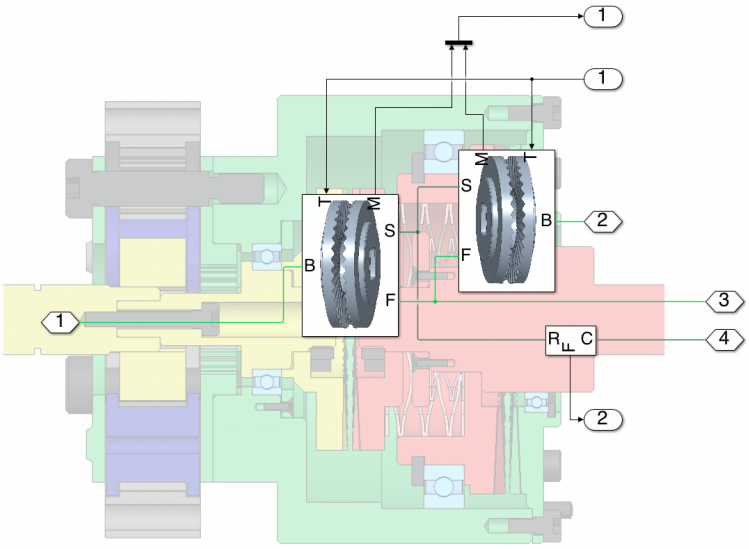


| | |
|---|---|
| Tutor: | M. Sc. Alexander Kirst |
| | Dipl.-Ing. Jens Reinecke |
| Supervisor: | Prof. Dr. techn. Klaus Janschek |
| Day of Submission: | 31.08.2021 |

STUDENT RESEARCH THESIS

Author: Julia Richter

# Contents


**1 Introduction** **1**
1.1 Background: The Switch-able Gear . . . . . 1

**2 State of the Art** **5**
2.1 Simulating Gear Clutches . . . . . 5
2.2 Humanoid Running . . . . . 7
2.3 Translational Actuators . . . . . 10
2.3.1 Requirements for the Shifting Actuator . . . . . 10
2.3.2 Lead and Ball Screws . . . . . 10
2.3.3 Cam Mechanisms . . . . . 11
2.3.4 Snapping Mechanism . . . . . 12
2.3.5 Other Variants . . . . . 13

**3 Requirements Definition** **15**
3.1 User Specifications . . . . . 15
3.2 Structural Analysis . . . . . 15
3.2.1 Context Analysis . . . . . 15
3.2.2 Data Flow Analysis . . . . . 17

**4 Design of the Simulation** **19**
4.1 Short Introduction to Simulink® and Simscape™ . . . . . 19
4.2 Basic Structure . . . . . 20
4.3 Transfer of Rotation with the Hirth Clutch . . . . . 23
4.3.1 Kinematic Analysis . . . . . 23
4.3.2 Modelling of Rotational Behaviour . . . . . 27
4.3.3 Modelling of Translational Behaviour . . . . . 27
4.3.4 Parameters of Simulated Hirth Clutch . . . . . 29
4.4 Movement of the Shifting Shaft . . . . . 31
4.5 Derivation of Input Data . . . . . 32
4.5.1 Data of Application . . . . . 32
4.5.2 Data for the Shifting Actuator . . . . . 34
4.5.2.1 Calculations for Lead Screw Mechanism . . 34
4.5.2.2 Calculations for Cam Mechanism . . . . . 36
4.5.2.3 Calculations for Snapping Mechanism . . . 37

**5 Validation** **39**
5.1 Scenario One: Slow Movement of Shifting Shaft . . . . . 40
5.2 Scenario Two: Fast Movement of Shifting Shaft . . . . . 41
5.3 Scenario Three: Decoupled Output Torque . . . . . 42

**6 Results** **43**
6.1 Lead Screw Mechanism . . . . . 43
6.2 Cam Mechanism . . . . . 45
6.3 Snapping Mechanism . . . . . 47
6.4 Recommendation of One Shifting Variant . . . . . 48
6.5 Influence of Shifting Time . . . . . 49

**7 Summary and Future Work** **51**

**Appendix A Specifications of the Shifting Actuator** **55**

**Appendix B Short User Guide for the Simulation** **57**

**Appendix C Further Calculations** **59**
C.1 Derivation of the Values for a Specific Cam Mechanism . . . 59

**References** **63**

# List of Figures


1.1 Scheme of a planetary gear . . . . . 2
1.2 Sectional view of the new switch-able gear . . . . . 3
1.3 Partly cut Hirth Serration . . . . . 4
1.4 Position of the shifting shaft for the two gears . . . . . 4

2.1 Biped TORO . . . . . 7
2.2 Detailed phases of the gait . . . . . 8
2.3 Joint data for human running . . . . . 9
2.4 Ball and lead screws . . . . . 11
2.5 Different cam mechanisms . . . . . 12
2.6 Schematic sketch of snapping mechanism . . . . . 12

3.1 Context diagram . . . . . 16
3.2 Data flow diagram: level a . . . . . 18

4.1 Description of the line colours in Simscape . . . . . 20
4.2 Range of translation of the shifting shaft . . . . . 21
4.3 Objects of F0 (screen shot of Simulink object diagram) . . . 22
4.4 Cut through Hirth serration shortly before contact . . . . . 23
4.5 Teeth contact dynamics . . . . . 24
4.6 Acting forces at teeth contact . . . . . 25
4.7 Structure of simulated Hirth clutch with object *Logic-Controlled Clutch* and separately modelled axial force . . . . . 28
4.8 Flow chart of trajectory calculation . . . . . 32
4.9 Input plots for simulation . . . . . 33

5.1 Output data for a functioning gear . . . . . 39
5.2 Output data for a too slow translation of the shifting shaft . 40
5.3 Output data for a too fast translation of the shifting shaft . 41
5.4 Output data for a decoupled output torque . . . . . 42

6.1 Output data for the lead mechanism . . . . . 44
6.2 Output data for the cam mechanism . . . . . 46
6.3 Output data for the snapping mechanism . . . . . 47

6.4 Measured angular velocity for inopportune switching . . . . 50

# List of Tables


3.1 Data lexicon: level 0 . . . . . 16
3.2 Data lexicon: level a . . . . . 18

4.1 Relevant settings for simulation of the Hirth serration . . . . 30
4.2 Assumed values for calculation of lead screw mechanism . . 36
4.3 Assumed values for calculation of a cam mechanism . . . . . 37
4.4 Assumed values for calculation of a snapping mechanism . . 38

6.1 Comparison of results from different shifting variants . . . . 48

A.1 Specifications of translational actuator . . . . . 55

# Nomenclature

## Abbreviations

| | |
|---|---|
| CAD | Computer-aided design |
| DAE | Differential algebraic equation |
| DLR | German Aerospace Center ('Deutsches Zentrum für Luft- und Raumfahrt') |
| ODE | Ordinary differential equation |
| PGT | Planetary gear transmission |
| TORO | Torque-controlled humanoid robot |

## Symbols

| | |
|---|---|
| $\alpha_{lead}$ | Angular acceleration of lead screw |
| $\ddot{\phi}_{rel}$ | Relative angular acceleration between two serrations |
| $\ddot{x}_A$ | Axial acceleration of shifting shaft |
| $\dot{\phi}_{rel}$ | Relative angular velocity between two serrations |
| $\dot{x}_A$ | Velocity of shifting shaft |
| $\dot{x}_N$ | Velocity in normal direction |
| $\eta$ | Efficiency |
| $\gamma$ | Half tooth flank angle |
| $\mu$ | Sliding friction coefficient |
| $\omega_M$ | Angular velocity of motor |
| $\phi_{rel}$ | Relative angular displacement between two serrations |
| $\rho$ | Sliding friction angle of lead screw |
| $\tau_{inertia}$ | Torque resulting from inertia to be rotationally moved |
| $\tau_{mass}$ | Torque resulting from mass to be translationally moved |
| $\tau_{max}$ | Maximum motor torque |
| $\tau_{nom}$ | Nominal motor torque |
| $\tau_{output}$ | Externally applied torque on shifting shaft |
| $\varphi$ | Pitch angle of lead screw |
| $a_{max}$ | Maximal possible acceleration of shifting actuator |
| $c_A$ | Stiffness in axial direction |
| $c_N$ | Normal stiffness |
| $c_{spring}$ | Stiffness of spring installed on shifting shaft |
| $c_T$ | Stiffness in tangential direction |

| | |
|---|---|
| $D$ | Outer radius of serration |
| $d$ | Inner radius of serration |
| $d_S$ | Pitch diameter of lead screw |
| $d_N$ | Normal damping |
| $F_{A,\tau}$ | Axial force resulting from torque at output |
| $F_{A,f}$ | Axial force resulting from friction force |
| $F_{A,N}$ | Axial force resulting from normal force |
| $F_f$ | Friction force |
| $F_{max}$ | Maximal force applicable by the shifting actuator |
| $F_N$ | Normal force |
| $F_{shiftingshaft}$ | Externally applied force on shifting shaft |
| $F_{T,f}$ | Tangential force resulting from friction force |
| $F_{T,N}$ | Tangential force resulting from normal force |
| $I_M$ | Inertia of motor |
| $I_s$ | Inertia of shifting shaft including serrations |
| $I_{lead}$ | Inertia of lead screw |
| $m_s$ | Mass of shifting shaft including serrations |
| $m_{lead}$ | Mass of lead screw |
| $p_h$ | Lead pitch of lead screw |
| $P_{in}$ | Input power |
| $P_{out}$ | Output power |
| $R_{eff}$ | Effective radius of the Hirth serration |
| $t_s$ | Shifting time |
| $v_{max}$ | Maximal possible velocity of shifting actuator |
| $x_0$ | Clearance between teeth when in idle mode |
| $x_A$ | Relative axial displacement of shifting shaft |
| $x_{N,A}$ | Displacement in normal direction resulting from axial displacement |
| $x_{N,T}$ | Displacement in normal direction resulting from tangential or angular displacement |
| $x_N$ | Displacement of teeth in normal direction |
| $x_{s0}$ | Pre-tensioned displacement of the snapping mechanism |
| $x_T$ | Relative displacement of teeth in tangential direction (resp. angular direction) |

# 1 Introduction

New applications require new technologies. Especially in the field of robotics, there are currently many challenges that cannot be realised with existing components. One institute that deals with these challenges is the Robotics and Mechatronics Centre at the German Aerospace Centre (DLR - Deutsches Zentrum für Luft- und Raumfahrt). This student thesis was written there.

Last semester, the author took part in the development of a new switch-able gear, presented below. The motivation behind the gear is to improve the walking behaviour of humanoid robots and to enable a dynamic running. Different applications are supposed to be possible as well. Concept-wise, the rotational movement transfer of the gear is already completed, but the drive that realises the actual shifting has not been designed. For the development of this actuator, it is important to be able to estimate the shifting behaviour of the gear and for this, a simulation is necessary.

After explaining how the new shift-able gear works, various solutions for the shifting actuator are presented. The subsequent requirements definition clarifies the general conditions of the simulation before the specific design is discussed in more detail. After validating the simulation, the results are presented, including a conclusive design recommendation for the shifting actuator.

## 1.1 Background: The Switch-able Gear

The term "switch-able gear" has two different meanings. In this thesis, it is used for shifting between different gear ratios and not for engaging and disengaging a certain part of the drive train.

The basic idea behind the development of the new switch-able gear was the need for a gear, which has the following characteristics:

- same rotational axis of input and output
- ability of gear-shifting without stopping the drive
- same behaviour in both rotational directions
- gear ratio above two

Research has shown that a gear which fulfils all four requirements does not yet exist.

One widely used gear in general is the planetary gear transmission (PGT). As shown in Figure 1.1, a PGT consists of a central gear wheel (sun), one internal gearing (ring) as well as a number of smaller gear wheels circling the sun inside the ring (planets). They are attached to the carrier, which has the same rotational axis as the sun and the ring. Of these three components (sun, ring, carrier) usually one is fixed, one is the input and one the output. However, either one could fulfil either task, so by simply changing the combination, different ratios are possible.

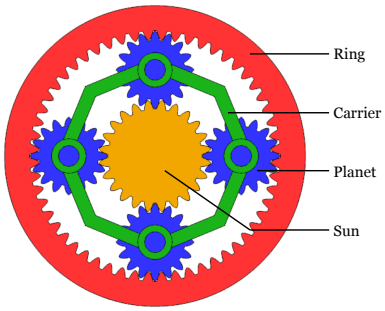


**Figure 1.1:** Scheme of a planetary gear with added legend. [Jah]

Even though the classic PGT is not able to switch between ratios, simple modifications can enable shifting ([Bec+20], [Kai93], [Sch18]). The new switch-able gear uses an approach were the ring is fixed, the sun is the permanent input and the output changes between sun and carrier. As a result the gear ratio can either be 1:1, if the sun is both the input and the output, or 4:1, when the sun is the input and the carrier the output.

In Figure 1.2 a sectional view of the new gear is shown. Part (*5*) is the ring, which is fixed with screws to the casing to inhibit movement in any direction. The sun (*2*) and the planets (*3*) usually have teeth, like the ring has, which are not part of this CAD file. The output shaft is not included in the picture. Instead (*10*) is the shifting shaft, which is rotationally connected to the output, but allows a small axial movement between these two parts.

The shifting between gears is realised with a modified Hirth clutch. In Figure 1.3 a closer view of its serration can be seen. It consists in general of two face serrations, which fit exactly on top of each other and guarantee self-centring [Vog47]. For the switch-able gear, two different sized clutches are used. The bigger one ((*8*) and (*9*)) connects the output to the carrier

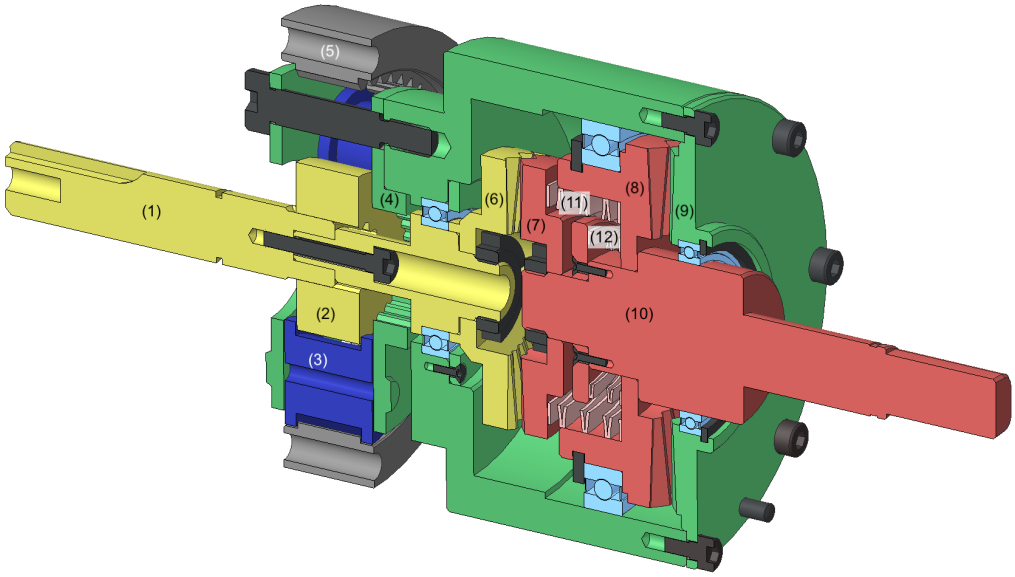


**Figure 1.2:** Sectional view of the new switch-able gear with added numbers. Parts coloured in the same colour have the same rotational speed. The emphasized parts are: (*1*) input shaft, (*2*) sun, (*3*) planet, (*4*) carrier, (*5*) ring, (*6*) Hirth serration for sun on input side, (*7*) Hirth serration for sun on output side, (*8*) Hirth serration for carrier on output side, (*9*) Hirth serration for carrier on input side, (*10*) shifting shaft, (*11*) large spring, and (*12*) small spring.

whereas the smaller one ((*6*) and (*7*)) does the same for the sun. Of the two pairs of Hirth serrations, respectively one partner is referred to as the input ((*6*) and (*9*)) and the other one as the output ((*7*) and (*8*)). The input is connected to the according part of the PGT both rotational and translational. The output is rotationally connected to the shifting shaft, but is able to move translational. This is made possible by matching polygon profiles on both shaft (*10*) and hub ((*7*) or (*8*)).

The coupling procedure itself can be seen in Figure 1.4. If the shifting shaft is moved to the right, the two larger Hirth serrations connect and allow a rotational transmission from the carrier to the output. If the shaft is moved to the left, the clutch of the carrier disengages and allows the one on the sun to engage. This results in a rotational transmission from the sun to the output.

The PGT assembled in this switch-able gear has a ratio of 4:1 between sun and carrier. Thus, the rotational speed difference between the serration

of the shifting shaft and the matching serration of the PGT can be rather high. Accordingly, there is a vast impact on the teeth while shifting. To reduce the risk of damage, springs or dampers allow a small movement of the output serrations to the shifting shaft. This is supposed to lead to an alternating engaging and disengaging within the shifting process until the different rotational speeds adjust and the Hirth spines engage completely. In Figure 1.2 two springs are used. The Hirth serrations for the sun is cushioned by (*11*) and the one for the carrier by both (*11*) and (*12*).

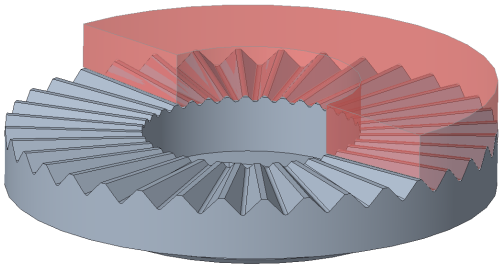

**Figure 1.3:** Partly cut Hirth Serration

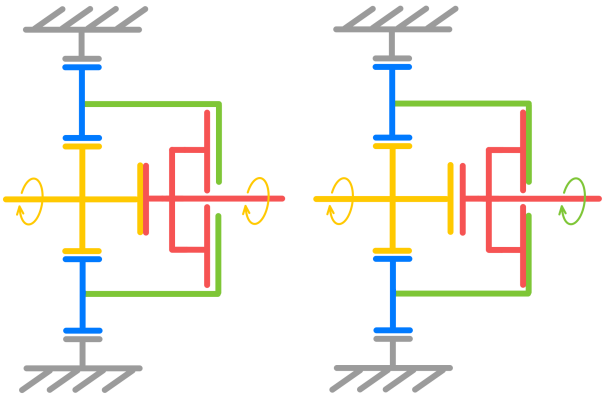

**Figure 1.4:** Position of the shifting shaft for the two gears

# 2 State of the Art

This chapter will first look into common methods for the simulation of gearboxes. One possible application for the new switch-able gear is humanoid walking. Therefore, a deeper look at this example is taken and a brief overview of the technical development in this field is given. Since the goal of this work is to further the development of the actuation, this chapter concludes with a presentation of commonly used translational actuators.

## 2.1 Simulating Gear Clutches

An important aspect of the development of new technologies are all kinds of simulations. They can be used to predict the behaviour of a system and to help with the decision-making process if there are different solutions for a certain problem. In case of the new switch-able gear an actuator, which moves the shifting shaft to the two end positions, needs to be developed. Since the dynamics of the gearbox are not yet known, there are no characteristic values that can serve as a reference within the designing process. Therefore, a dynamic simulation of shifting process of the switch-able gear is required.

Simulations are always only a representation of the real world. They are built-up of mathematical equations and physical relations, which can be graphically represented in different ways. One typical approach are signal oriented block diagrams, whereby a signal flows between causal blocks. However, in physical systems it is often difficult to define the direction of these signals. A solution for this problem are object diagrams. They divide systems into their components and display the relation of these. The lines between two components are bidirectional and are defined as an actual physical connection. Points where several lines meet, called ports, define an interaction. From a physical view the lines are interpreted as energy flow. In all physical domains, whereas domains are for example translational dynamics or electric circuits, the power can be described as the product of two variables: the effort and the flow variable. At the interaction points, all flow variables sum up to zero. On any closed path, the sum of all differences of the effort variables is zero. For mechanical systems an interaction point is a flange. The effort variable is the velocity, since all objects connected to

the flange have the same velocity. The flow variable is accordingly the force. [OSE97] [Eno11] [Pie08]

Nowadays there are several comfortable object diagram editors with easy-to-use graphical user interfaces. Examples for editors are Dymola, which is based on the Modelica modelling language, or Simulink® with the extension Simscape™. Both offer many ready-made objects - basic objects, such as springs and dampers, as well as advanced, such as clutches. However both do not include a Hirth coupling.

The reason is probably the following: Hirth serrations are commonly used for static coupling (compare [Lin18, p. 282], [Hab18, p. 406], [Vog47]). The two halves are connected while standstill and are translational fixed for example by screws. Afterwards the drive starts and a rotational movement can be transmitted. For the new switch-able gear the Hirth serrations are supposed to connect dynamically without stopping the rotational motor. This makes the simulation quite challenging. To the best of the authors knowledge, the Hirth serration has not been used in the described way. Hence, no experimental data is available, which could help building the simulation. Instead the focus here is on similar problems and their solving.

Most existing simulations focus on advancing drive-trains or complicated set-ups, such as automotive transmissions ([OSE97], [Zha+14], [Jia+11]). There are only few models for the simple shifting process of gears. One similar gear to the Hirth clutch are dog clutches, which Duan simulated [Dua14]. Duan divides the physical model into the domains rotational dynamics and translational dynamics. The according effort variables are translational and angular velocity and the flow variables respectively force and torque. The physical equations are separately calculated and connected through the normal force of the tooth, which applies to both dynamics. Bóka has a similar approach but for the axial sliding of axial splined dog clutches [Bók+10]. An additional focus is placed on the friction loss between the sliding teeth. Further relevant examples could not be found.

## 2.2 Humanoid Running

**Figure 2.1:** Biped TORO [DLR]

One possible application for the new switch-able gear is the already mentioned humanoid running. The specific application is the knee joint of DLR's TORO (torque-controlled humanoid robot) shown in Figure 2.1. Instead of muscles and tendons like a human, TORO, similar to many other bipeds ([Hir+98], [LTZ07]), has a servo motor in the knee joint that initiates a movement between the thigh and the lower leg. Just like TORO, these robots are so far unable to reach high locomotion speeds. To the best of the authors' knowledge, the only faster robot is Atlas by Boston Dynamics [Dyn]. However, it has hydraulic joints instead of electric ones, which limits its field of application because of pressure- and temperature-dependency. There are only a few approaches to make electrically driven bipeds faster. One approach is DLR's C-Runner, in which mechanical springs act as an energy buffer and thus enable more efficient running [Loe+16]. Another idea, described in the following, was pursued in the development of the switch-able gear.

The principle is to reduce the required motor power for a dynamic gain by dividing the gait cycle into two parts: the stance phase and the swing phase, each of which is defined for one leg and can be comprehended in figure 2.2 for the human example. The stance phase is the part of the gait cycle in which the leg is in contact with the ground. Here the entire weight of the body rests on one leg, which leads to a high torque in the robotic knee joint. The swing phase is the period in which the foot does not touch the

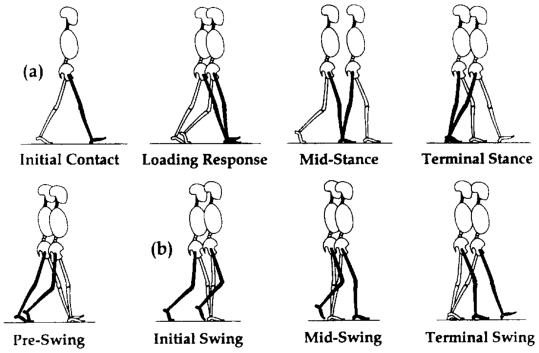


**Figure 2.2:** Detailed phases of the gait with a) stance and b) swing phase [Bek+92, p. 294]

ground. This relieves the robotic knee joint and a significantly lower torque is required. The foot is swung forward quickly, which on one hand contributes to stabilisation and on the other hand enables a dynamic movement. Hence, a rather fast angular velocity is required here. [Per92]

Figure 2.3 shows plots for different parts of the human gait apparatus within the gait cycle. The important column here is the middle one, which displays the plots for the knee joint. The solid line is the data for running. All plots are plotted over time, more precisely the progress of the gait cycle in percent. The end marks 100%, which corresponds to 1 s. The first plot shows the behaviour of the angle between the thigh and lower leg. Zero means the leg is fully extended and a positive angle is the according flexion. The vertical line marks the point of foot-take-of and thus the transition from stance into swing phase. The first apparent peak is the slower flexion while load response. The second peak is the faster flexion in preparation for the forward swing. The second graph of Figure 2.3 is the acting torque within one gait cycle. It is normalized by body weight in kilograms. The first peak is the load response with a rather high acting torque of 1.6 N m· *bodyweight*/kg. In the further course the torque is rather low with stable 0.2 N m · *bodyweight*/kg from 40% to 60% and -0.5 N m · *bodyweight*/kg at the end of the gait cycle. [Nov98]

This data can not be transferred directly to a humanoid robot. However, it roughly indicates the order of magnitude to be expected. This is sufficient for simulation and to make a recommendation for the design of the shifting actuator. Before the simulation as well as the gear in general can be adapted to a biped, specific data from robotics must be available.

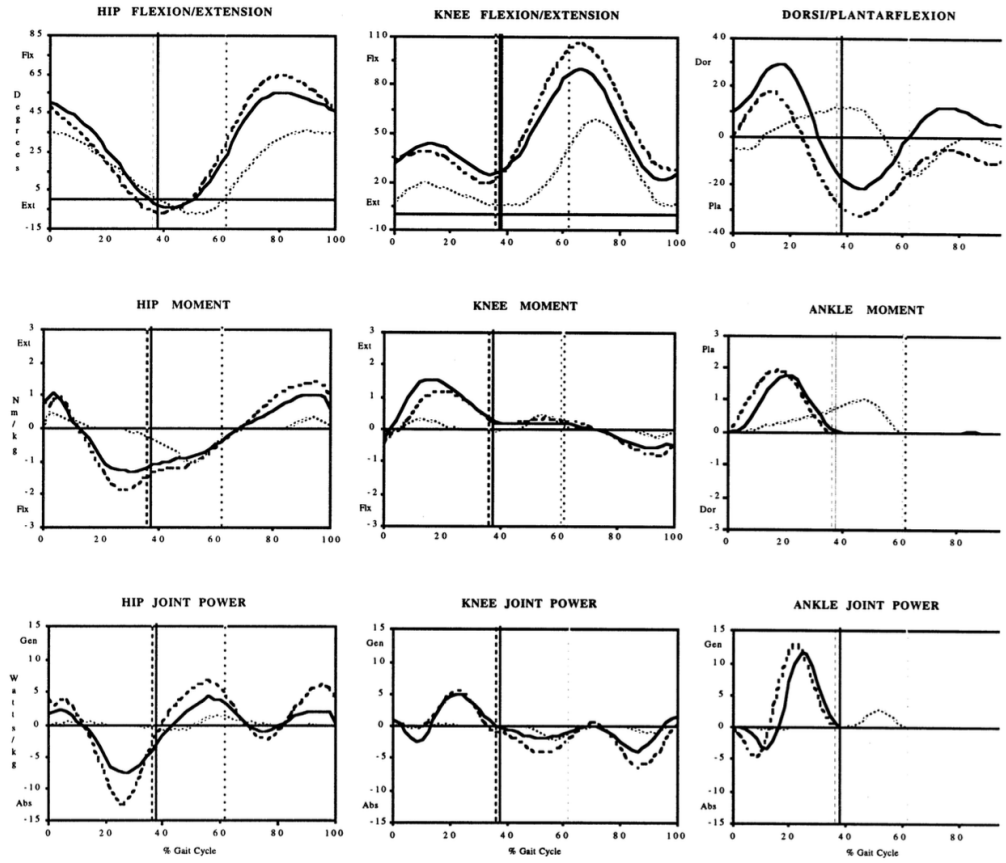


**Figure 2.3:** Joint data for human running: Joints are organized by column. Within one column first the angle of the according joint is plotted, then the torque and last the power - all plotted over the course of one gait cycle in %. [Nov98, p. 86]

## 2.3 Translational Actuators

This section will take a look at already existing technologies for translational movement. At the beginning, a catalogue of requirements is drawn up in relation to the switch-able gear presented in the beginning. Thereafter, different variants are discussed.

### 2.3.1 Requirements for the Shifting Actuator

Since the actuator to be developed must be adapted to the existing switch-able gear, some requirements are imposed. A comprehensive table can be found in Appendix A. The main aspects are now summarised.

Firstly, the geometry needs to fit the gear to enable an integrated assembly. For that it has to have the same cylindrical form with a maximum diameter of 77 mm and a hollow space in the middle with minimum 25 mm diameter. The shifting shaft is supposed to fit into the actuator and rotate freely in relation to it. As common in the field of robotics, the new construction has to be as light as possible. Concerning kinetics and kinematics, the shifting shaft needs to move, depending on specific design, between 4 mm and 8 mm. For the humanoid running application, the gear has to shift twice within one gait cycle, which compromises 1 s. Hence, the actuator has to be fast enough to cover the distance within 500 ms, preferably in less than 100 ms. The force generated when engaging depends on the shifting dynamics and can thus not be defined beforehand. It has to be checked after the simulation was established. Lastly the actuator, as the gear, has to have a wide range of applications especially concerning extreme environmental influences.

### 2.3.2 Lead and Ball Screws

A drive, which fulfils the geometric requirements is a servo motor. It has to be combined with a mechanism to change the rotational to a translational movement. Since the requirements include a hollow cylindrical shape, the most practical construction involves a hollow motor in which the shaft is mounted. Hence, the direction of translational movement has to be the rotational axis of the motor. This excludes many common mechanisms.

One approach for this transfer is a lead screw, which can be seen in Figure 2.4a. It combines a threaded rod with a nut screw. If the rod is rotated while the nut can not turn, a translational movement results. However, since the surfaces rub against each other, the efficiency is below 40% [SDP14, p. 26].

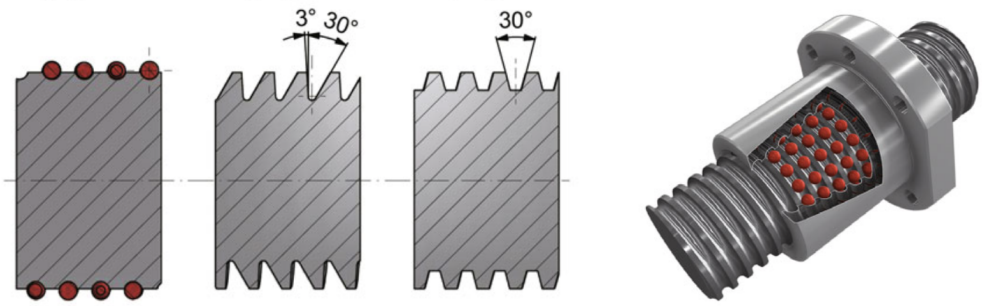


**(a)** Comparison of different screws [SDP14] **(b)** Ball screw [SDP14]

**Figure 2.4:** Ball and lead screws

The common alternative is a ball screw in Figure 2.4b. It reduces friction by placing small balls in the gaps that transmit the movement. However, they must not be subjected to shock loads as these will damage the mechanism [SDP14, p. 71], This can not be guaranteed in the targeted application. Therefore, only the lead screw is considered.

### 2.3.3 Cam Mechanisms

A further idea is a variant of a cam mechanism in combination with a servomotor. Similar to a cam disk, a certain geometry is given, which leads to a certain motion when a rotation is applied. The main difference of the considered variant is the working direction, which is axial to the rotation instead of radial. The two variants here discussed are (a) cylindrical or barrel cam and (b) end cam. Both can be see in Figure 2.5. The cylindrical cam consists of a cylinder in which the trajectory is cut into. The example in Figure 2.5a has only one path with one roller inside. However due to better force distribution, it is advisable to use two or three parallel paths. The roller is fixed to the so called follower, which is fixed against rotation. Hence, a rotation of the cylinder leads to a translational motion of the follower - similar to the lead screw, but more efficient but less flexible instead.

In some cases it is more practical to use a end cam mechanism, seen in Figure 2.5b. It consists of two plates, of which one has a curved profile and is connected to the servomotor. The other has rollers attached, which roll on the curved surface, and is rotationally fixed. The mechanism works similar to the cylindrical cam. If the curved plate is rotated, the rollers roll onto the next stage, leading the flat plate to a translational motion. In contrast to the

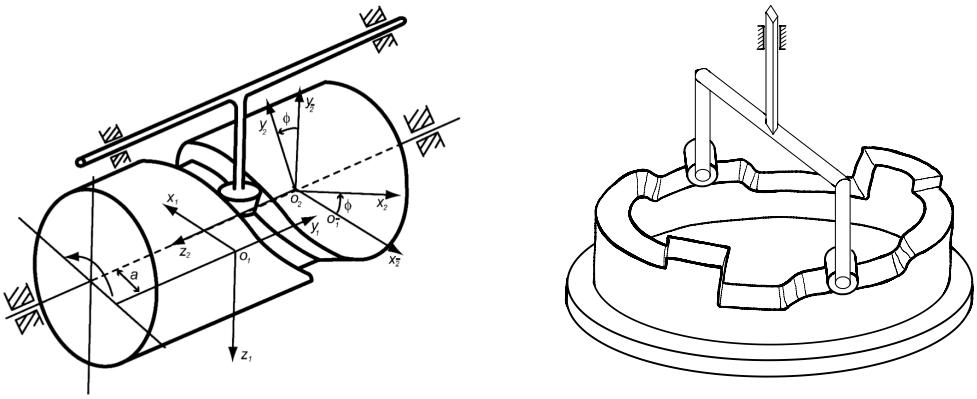

**(a)** Cylindrical cam [Pez+05]

**(b)** End cam with three stages and two rollers

**Figure 2.5:** Different cam mechanisms

cylindrical cam, springs are required for the end cam to hold the two plates together, if this task is not taken over by gravity. Because of the springs, an additional force has to be applied to realise the movement. Otherwise the calculation is the same as for the cylindrical cam.

### 2.3.4 Snapping Mechanism

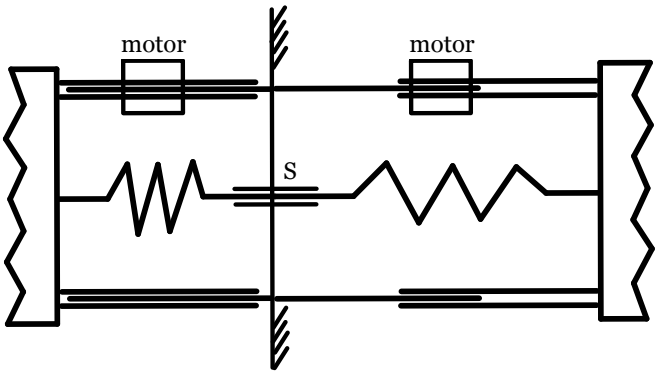


**Figure 2.6:** Schematic sketch of snapping mechanism, where the left side (Hirth sun) is tensioned and the right side (Hirth carrier) is relaxed and $S$ marks the shifting shaft.

Another possibility to be presented here is a snapping mechanism. The general idea is to use two springs to realise the translational movement. For the shifting process either one of the previously tensioned springs is released and thus induces a fast displacement of the serration on the shifting shaft. When the other spring is released to move the other serration in the other direction, the first spring is slowly tensioned again. Figure 2.6 shows the working principle. Here the left side is tensioned and the right side is released. The serrations move respectively relative to the shifting shaft S, which is fixed in translational direction. In addition to the springs, the illustration shows rails on which the serration is beared. This variant requires two motors, which need to have significantly less power than in the previous variants.

### 2.3.5 Other Variants

The simplest approach for a translational actuation is a linear motor. It combines fixed permanent magnets and electromagnets, which are able to move alongside the former. A constantly reversing polarity of the electromagnets leads to a magnetic attraction and repulsion of the two components and thus to the translational movement [Kal+18, p. 246ff]. Solenoids have an similar approach. The configuration is changed, so that the electromagnet is fixed and the permanent magnet moves along it [Kal+18, p. 313f]. Both variants have the disadvantage that magnets have a smaller actuating force when a longer distance needs to be covered [Lin18, p. 642]. Furthermore, permanent magnets are in general rather heavy if higher forces are required [Kal+18, p. 248]. Since the gear should be as minimalistic as possible, they are not applicable.

Another rather new approach are piezo-electrical actuators. They make use of the piezo-electrical effect, which states that solids can deform under the impact of an electrical field or the other way around that a deformation of solids can induce an electrical field. The translational actuator uses the primer part of this phenomenon. When applying an electrical field, the average piezo-electrical actuator can elongate up to a permille of its own length [Lin18, p. 643ff]. For an actuator with the length of 50 mm, the elongation is accordingly 50 µm. This elongation is far to small for the application and thus excluded.

Besides the already mentioned, pneumatic or hydraulic actuators are quite common. They have many advantages, such as a small installation space for the actual power generation since the tank and the pump for pressure build-up can be at a different place of the machine [Lin18, p. 660f]. However, as

already explained in the previous chapter, the use of a fluid or gas brings the disadvantage of pressure- and temperature-dependency. Even though the introduced application is humanoid walking, the gear is also meant to be a basic technology. While the stated dependencies are not a major problem on Earth, they may bring complications under extreme environmental conditions or even in space. This is contrary to the requirements and thus hydraulic and pneumatic actuation are excluded.

In conclusion, the selection of a shifting actuator remains with the three variants first described.

# 3 Requirements Definition

This chapter deals with an overlook of the simulation. First, a user requirement is given, which highlights the goal of the simulation. Then the structured analysis of the problem is presented. This is divided into two parts: the context analysis and the data flow analysis.

## 3.1 User Specifications

The simulation is developed to optimise the development process of a shifting-shaft actuator for the new shift-able gear. This drive is to be developed for a specific application, which may change during the development process or later. Therefore, the parameters of this application are a relevant input. As a result of the simulation, the engineer of the shifting actuator receives data that helps him with the development of the drive.

## 3.2 Structural Analysis

This user specification is followed by the context diagram in which the terminator is defined and how it related to the simulation. The data flow analysis thereafter goes into more detail about the different functions and what data flows between them.

### 3.2.1 Context Analysis

On the right side of Figure 3.1 the main function "*simulate* switch-able gear" (F0) can be seen. The user starts the simulation via the control flow D0.1. Since the gearbox is to be designed for a special application, two values (D0.2 and D0.3) are required from this application. One is the rotational velocity (D0.2) that the output is supposed have. Secondly, the torque (D0.3) is entered, which acts as a disturbance variable on the simulated gear performance. Both are given as plots and are sampled in the course of the simulation. D0.4 is the gear selection, which is manually derived from the two given graphs. To simulate the translational actuation, the boundaries of the shifting actuator (D0.5) are given as well. They include the maximum

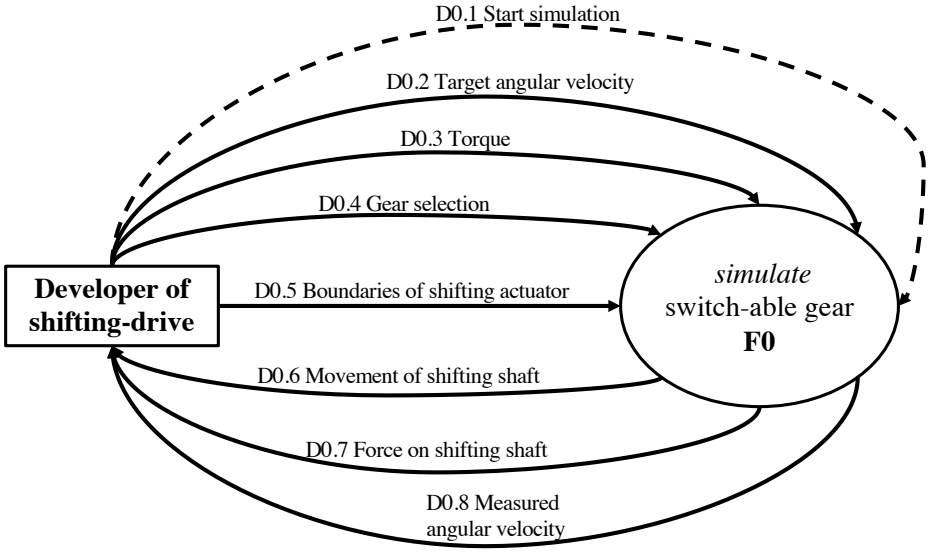


**Figure 3.1:** Context diagram

**Table 3.1:** Data lexicon: level 0

| | **Name** | **Further explanation** |
|---|---|---|
| D0.1 | Start simulation | |
| D0.2 | Target angular velocity | needed at output side of gear |
| D0.3 | Torque | applied at output side of gear |
| D0.4 | Gear selection | discrete value [gear 1, gear 2, idle] |
| D0.5 | Boundaries of shifting actuator | $a_{\max}$, $v_{\max}$ |
| D0.6 | Movement of shifting shaft | measured velocity and position |
| D0.7 | Force on shifting shaft | measured force |
| D0.8 | Measured rotation | angular velocity at output side of simulated gear |

translational velocity and maximum translational acceleration that the actuator can deliver. As a result of the simulation, the user receives three plots. The movement of the shifting shaft (D0.6) and the force (D0.7) are the parameters required to develop the shifting actuator. The measured angular velocity (D0.8) is used to check if the simulation has worked properly.

The terminator is the engineer, who is supposed to design the shifting actuator. He provides the application data and boundary conditions for the shifting actuation. He starts the simulation and receives the data required for the designing. For monitoring purposes, he also receives the simulated output of the gear to see if the chosen boundary conditions have been successful.

### 3.2.2 Data Flow Analysis

In Figure 3.2 the main function is shown in detail. The simulation starts with F1, which translates the target gear given by the user to the according position Da.1. This position flows to F2, which moves the shifting shaft to the designated position. For this movement, the boundaries are given by D0.5. The movement of the shifting shaft is measured and given back to the user via D0.6. The mechanical translation of the shifting shaft flows via Da.2 to F5.

F3 re-calculates the angular velocity depending on the gear selection, which flows into F3 from F5 via Da.3. For gear 2, with a gear ratio of 1:1, no re-calculation needs to be done. In gear 1, with a gear ratio of 4:1, the input angular velocity needs to be multiplied by 4 to achieve the correct angular velocity at the output. The corrected angular velocity flows via Da.4 to F4. Here the angular velocity, which up to now has only been a signal, is converted into a mechanical rotation. The outputs of F4 are Da.5 and Da.6, which are the mechanical rotations of the carrier (Da.5) and the sun (Da.6).

Both outputs of F4 are connected to F5, which connects the translational and rotational movement. Depending on the translational position of the shifting shaft, a certain angular velocity is transmitted from the inputs to the output. Data-wise this means that the mechanical rotation of the output (which equals the rotation of the shifting shaft) Da.7 is either the one of the carrier or the one of the sun. In between is a transition phase. The torque D0.3, which the output is subjected to, also flows into this calculation. Within F5 the axial force, which acts on the shifting-shaft, is calculated. D0.7 gives this value to the user. The other important output of F5 is the mechanical rotation of the output Da.7, which is measured by F6 and then displayed to the user via D0.8.

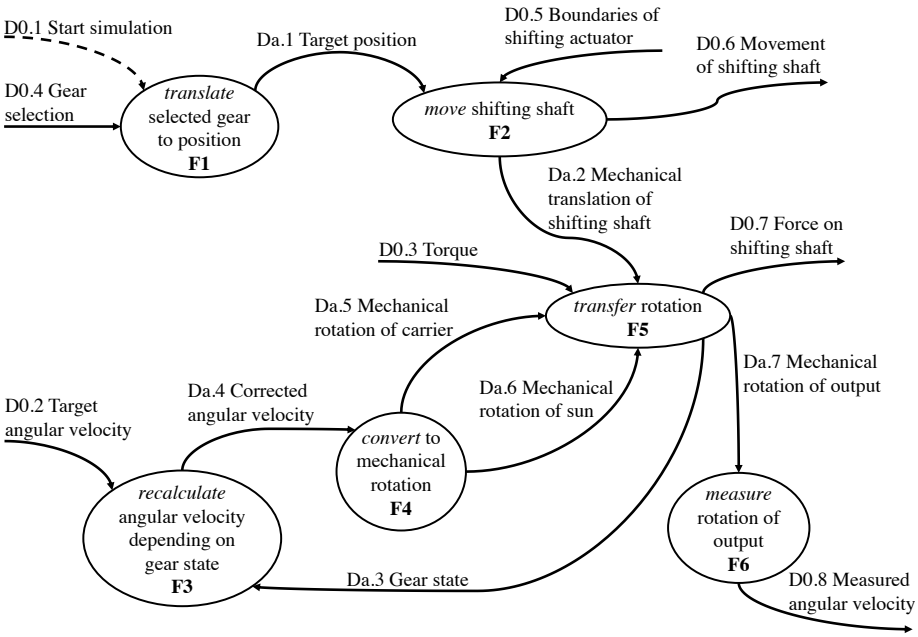


**Figure 3.2:** Data flow diagram: level a

**Table 3.2:** Data lexicon: level a

| | Name | Further explanation |
|---|---|---|
| Da.1 | Target position | relative axial position of shifting shaft to gear |
| Da.2 | Mechanical translation of shifting shaft | described by force and velocity |
| Da.3 | Gear state | gear that is currently engaged |
| Da.4 | Corrected angular velocity | applied at input of gear |
| Da.5 | Mechanical rotation of carrier | described by torque and angular velocity |
| Da.6 | Mechanical rotation of sun | described by torque and angular velocity |
| Da.7 | Mechanical rotation of output | described by torque and angular velocity |

# 4 Design of the Simulation

This chapter focusses on the simulation. At the beginning it gives a short introduction to the applied software, Simulink® and its extension Simscape™. Following it will look into the basic structure of the developed simulation and explain the different functions. The implementation of certain components of the gear is extensively discussed. Especially for the Hirth clutch, the motion equations are presented. In the end, the derivation of the input data is explained.

## 4.1 Short Introduction to Simulink® and Simscape™

For the simulation of the new switch-able gear, Simulink® was used. Simulink itself works with signal flows between components. Since the calculations behind the gearbox are quite complex, which limits a clear arrangement of the simulation, the Simscape™ extension was additionally used. It describes the energy flow between elements, as explained in Chapter 2.1. To distinguish between signal flows and energy flows, different line colours are used in Simscape, which can be seen in Figure 4.1. Black stands for the classic, unidirectional signal flows. Brown are physical signals, which are also unidirectional, but have a defined unit. Otherwise coloured lines are energy flows that run bidirectionally and thus have no arrows drawn in. Translational elements are light-green and rotational dark-green. To connect signal flows and energy flows, sources and sensors are used. With sources, the signal flow is first converted into a physical signal, which in turn serves as an input for a *Source* object. According to the flow and effort variables, either a velocity/ angular velocity or a force/ torque can be given into the mechanical system as a source. The counterpart to sources are sensors. They measure the flow or effort variable and output a physical signal, which again can be converted into a Simulink signal.

In addition to the sources and sensors there are a number of basic elements in the Simscape Foundation library. For translational motion, it includes among others springs and dampers. Behind these masks are the differential algebraic equations (DAE), which describe the behaviour of the elements. When running the simulation, an implicit DAE system is created, which is

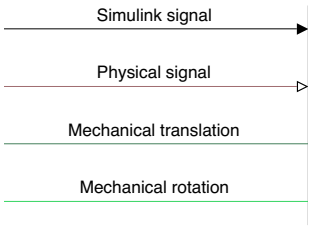


**Figure 4.1:** Description of the line colours in Simscape

then solved. Algorithmic details are described in [Pie08, p. 167]. In addition to the Simscape Foundation library, the Simscape Driveline library is also used in this work. It offers additional components, such as special clutches, which will be discussed later in this chapter.

Because of the implicit DAEs, an implicit solver is required. In the MathWorks Help Center on the side "Making Optimal Solver Choices for Physical Simulation" three possible Simulink solvers are named for systems with Simscape components: *daessc*, *ode15s* and *ode23t*. All three have a variable-step size and work for continuous simulations. Even if *daessc* was specifically designed for physical modelling, it is relatively new and only available for Simulink versions 2021a and above. To ensure that the simulation also works in older versions, it was decided against this solver. The difference between *ode15s* and *ode23t* is the stability and the capturing of oscillations [Mat]. The latter has a reduced stability, but does not damp out oscillations like the first. Since oscillations can not be excluded because of the usage of springs, *ode23t* was chosen. This solver uses the trapezoidal method for solving the implicit equations.

## 4.2 Basic Structure

The structure of the simulation is based on the structural analysis and can be seen in Figure 4.3. Within the main function "*simulate* switch-able gear" the objects are identical with the functions F1-F6 of the context diagram in Figure 3.1. The main difference is the partly usage of energy flow instead of signal flow. The data flow variable Da.2 changes from a data flow to an energy flow of mechanical translation and Da.5, Da.6 and Da.7 to mechanical rotation. Functions F2, F4 and F5 work as translators between the Simulink signals and the Simscape energy flows. F2 and F5 are explained in

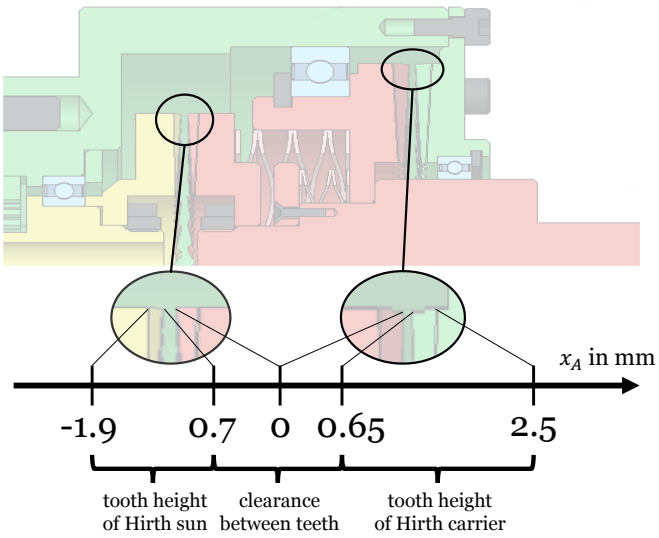


**Figure 4.2:** Range of translation of the shifting shaft with marked tooth height and clearance between teeth

more detail later in this chapter, while the other functions are now briefly described.

F1 translates the selected gear to the associated position. Figure 4.2 shows the according coordinate system. The shifting shaft starts at position 0 which marks the idle mode or gear 0, where neither clutch is connected. For gear 1, the clutch of the carrier is supposed to connect. Hence the shifting shaft is moved along the axis to position 2.5 mm. For gear 2, it is the same procedure but with the sun and the according position -1.9 mm.

Since gear 1, or the carrier-gear, has a ratio of 4:1, the input angular velocity has to be four times faster than the target velocity to meet the target at the output side. For this, F3 has the gear state, which F5 sets, as an input and makes the according change.

F4 translates this velocity with an *Ideal Velocity Source* to a mechanical rotation. This is connected to a planetary gear, which transmits the mechanical rotation from the input, respectively the sun, to the carrier. The outputs of F5 are the two mechanical rotations of sun and carrier.

After F5 transmits either one of these mechanical rotations to the output side, respectively the shifting shaft, F6 measures the rotation with an *Ideal Angular Velocity Sensor*. The resulting physical signal is translated to a Simulink signal and transmitted back to the user.

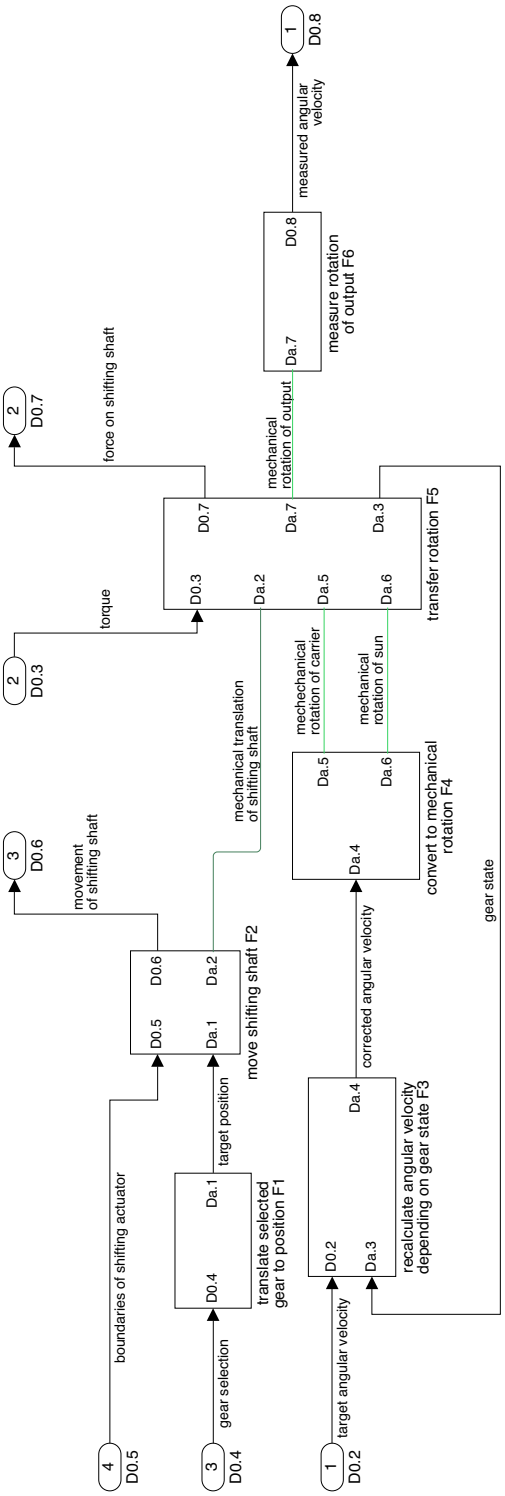


**Figure 4.3:** Objects of F0 (screen shot of Simulink object diagram)

## 4.3 Transfer of Rotation with the Hirth Clutch

The goal of F5 is the mechanical modelling of the dynamic transmission behaviour and thus the heart of the simulation. The physical input variables are the mechanical translation of the shifting shaft and the mechanical rotations of the sun and carrier. Another input is the signal variable of disturbance torque which is applied at the output side of the switch-able gear. In order to better understand the behaviour of the shifting process, the equations of motion are derived in the following section.

### 4.3.1 Kinematic Analysis

The difficulty of modelling a dynamic Hirth clutch, is the combination of rotational and translational movement. Because of the angle between the tooth flanks, every axially applied force results in a torque and vice versa. At this point, the expected coupling behaviour is briefly described. In contrast to conventional face serrations, the tooth height of the Hirth serration is not constant, but decreases in radial direction towards the centre. As a result, the teeth first meet at the tip at the outermost radius. Due to the practically non-existent contact surface, no clamping can occur. The clutch engages even if two teeth are in direct contact, as indicated in Figure 4.4.

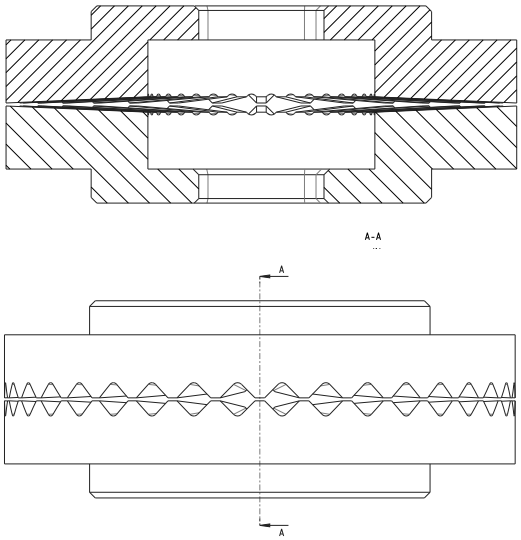


**Figure 4.4:** Cut through Hirth serration shortly before contact

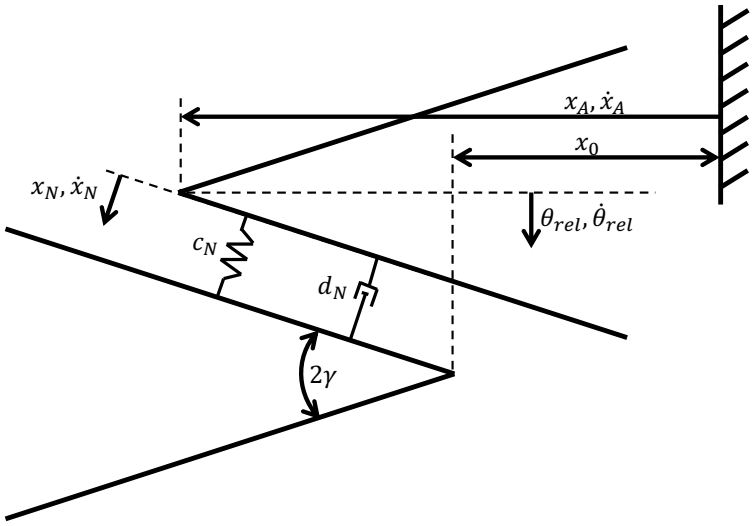


**Figure 4.5:** Teeth contact dynamics. Derived drawing from [Dua14]

When the Hirth clutch halves are pushed together dynamically, the teeth meet. The normal force created by the elastic impact response is divided into an axial force and a tangential force. While the axial force acts on the shifting shaft, the tangential force results in a torque, which acts on the Hirth clutch halves. Although this behaviour has not yet been analysed for Hirth gears, Duan deals with the dynamic behaviour of a dog clutch with pointed teeth [Dua14]. The described behaviour is also expected from the Hirth serration. Therefore, the paper mentioned serves as the basis for the following calculation.

Based on Duan [Dua14], at the moment of impact, the elastic displacement of the teeth is described by a spring-damping system, as shown in Figure 4.5 and described by

$$F_N = c_N \cdot x_N + d_N \cdot \dot{x}_N, \tag{4.1}$$

where $F_N$ is the normal force, $c_N$ the normal stiffness of the teeth, $x_N$ the displacement in normal direction, $d_N$ the normal damping and $\dot{x}_N$ the velocity of the displacement in normal direction. The normal displacement results from an axial displacement $x_A$ and tangential displacement which again results from the relative angular displacement $\phi_{rel}$ between two teeth.

The directions can be combined as

$$x_{N,A} = (x_A - x_0) \cdot \sin(\gamma) \text{ and} \tag{4.2}$$

$$x_{N,T} = R_{eff} \cdot \sin(\phi_{rel}) \cdot \cos(\gamma) \tag{4.3}$$

$$\text{with } R_{eff} = \frac{D+d}{4}, \tag{4.4}$$

where $x_{N,A}$ is the displacement in normal direction resulting from the axial displacement, $x_0$ the axial clearance when the teeth are disengaged, $\gamma$ the half tooth flank angle, $x_{N,T}$ the displacement in normal direction resulting from the angular displacement $\phi_{rel}$, $R_{eff}$ the effective radius, D the outer and d the inner diameter of the Hirth serration. The product $R_{eff}\sin(\phi_{rel})$ can be approximated for small angles to $R_{eff}\phi_{rel}$. This creates

$$x_N = (x_A - x_0) \cdot \sin(\gamma) + R_{eff} \cdot \phi_{rel} \cdot \cos(\gamma) \tag{4.5}$$

and therefore

$$\dot{x}_N = \dot{x}_A \cdot \sin(\gamma) + R_{eff} \cdot \dot{\phi}_{rel} \cdot \cos(\gamma). \tag{4.6}$$

According to the force triangle in Figure 4.6, the normal force $F_N$ is divided with the help of

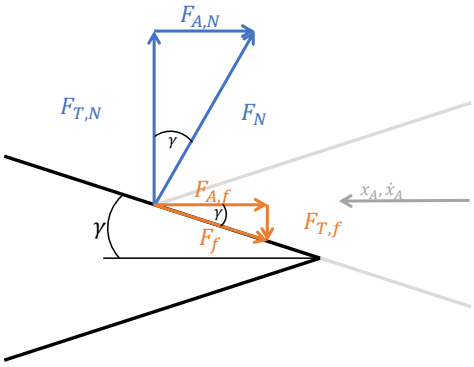


**Figure 4.6:** Acting forces at teeth contact

$$F_{A,N} = F_N \cdot \sin(\gamma) \text{ and} \tag{4.7}$$

$$F_{T,N} = F_N \cdot \cos(\gamma), \tag{4.8}$$

where $F_{A,N}$ is the axial force resulting from the normal force and $F_{T,N}$ the tangential force resulting from the normal force. Additionally a friction force $F_f$, resulting from the sliding of the teeth to each other, has to be included. The directions can be seen in Figure 4.6 and are calculated as

$$F_{A,f} = F_f \cdot \cos(\gamma) \cdot \text{sgn}(\dot{x}_A) \text{ and} \tag{4.9}$$

$$F_{T,f} = -F_f \cdot \sin(\gamma) \cdot \text{sgn}(\dot{x}_A) \tag{4.10}$$

with

$$F_f = F_N \cdot \mu, \tag{4.11}$$

where $F_{A,f}$ is the axial force resulting from the friction force $F_f$, $F_{T,f}$ the tangential force resulting from the friction force and $\mu$ the sliding friction coefficient. With this the axial and tangential force follows to

$$F_A = F_N \cdot (\sin(\gamma) + \mu \cdot \text{sgn}(\dot{x}_A) \cdot \cos(\gamma)) \text{ and} \tag{4.12}$$

$$F_T = F_N \cdot (\cos(\gamma) - \mu \cdot \text{sgn}(\dot{x}_A) \cdot \sin(\gamma)). \tag{4.13}$$

The resulting motion equations are

$$m_s \cdot \ddot{x}_A = F_{shiftingshaft} - F_A \text{ and} \tag{4.14}$$

$$I_s \cdot \ddot{\phi}_{rel} = \tau_{output} - F_T \cdot R_{eff}, \tag{4.15}$$

where $m_s$ is the mass of the shifting shaft with serration, $\ddot{x}_A$ the acceleration of the shifting shaft, $F_{shiftingshaft}$ the externally applied force on the shifting shaft, $I_s$ the inertia of the shifting shaft, $\ddot{\phi}_{rel}$ the angular acceleration of the shifting shaft including serrations, $\tau_{output}$ the externally applied torque on the shifting shaft and $R_{eff}$ the effective radius of the Hirth serration.

### 4.3.2 Modelling of Rotational Behaviour

As the previous chapter indicates, the movement of the gear can be decomposed into translation and rotation. The two parts are considered separately in the following, starting with rotation.

For a start, the libraries of Simulink were searched for components with a similar behaviour. In the Simscape Driveline library, the model of a face dog clutch with straight teeth is given in the object *Dog Clutch*. For straight teeth, the engagement process is abrupt. Furthermore the axial force that develops for Hirth serrations while torque is transmitted, does not arise. Hence, the behaviour does not match the one expected from the Hirth clutch.

Another modelling possibility would be a friction clutch. The Simulink Driveline Library offers the *Logic-Controlled Clutch*, a friction clutch that can be coupled in or out by an external input. The idea here is to base the logic on the shifting shaft displacement and thus connect the two shafts depending on the overlapping tooth height.

The decision thus had to be made between using the before derived equations or one of these two components. To make this decision, the two components were functionally tested. It was found that the *Dog Clutch* represents the engagement process well for certain parameter settings. However, the force while coupling-in strongly depends on the damping of the teeth. Since this value is not known for the Hirth serration and can not be figured out through a static FEM analysis, the behaviour of the simulation with the *Dog Clutch* too unreliable.

The *Logic-Controlled Clutch* behaves rotationally as would be expected from the Hirth clutch. Thus this variant was chosen. However, this object does not develop an axial force, since it does not include the domain *Physical translation*. The force had to be modelled separately, which is described in the next chapter.

### 4.3.3 Modelling of Translational Behaviour

There are two different phenomenons, which apply an axial force on the shifting shaft. First, there is a rather high jerk during the coupling process. This part can be calculated with the motion equations from Chapter 4.3.1.

Additionally, since the teeth of the Hirth clutch are triangular, an axial force develops while a torque is transmitted. It is calculated with [Rüt]

$$F_{A,\tau} = \frac{4 \cdot \tau_{output}}{D + d} \cdot \tan(\gamma), \tag{4.16}$$

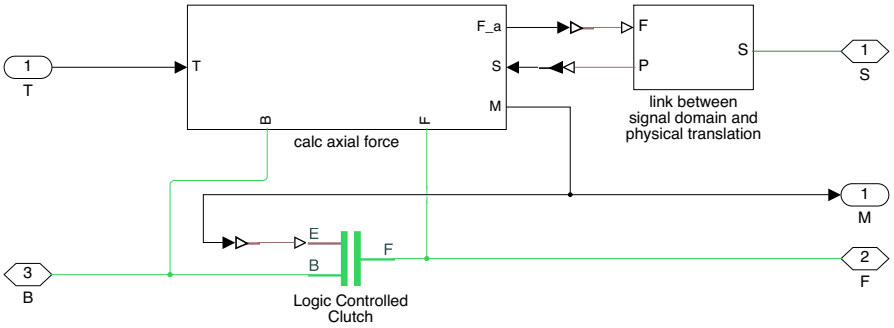


**Figure 4.7:** Structure of simulated Hirth clutch with object *Logic-Controlled Clutch* and separately modelled axial force

where $F_{A,\tau}$ is the axial force resulting from the transmitted torque $\tau_{output}$, $D$ the outer, $d$ the inner radius and $\gamma$ the half teeth flank angle. Both forces are not provided from the *Logic-Controlled Clutch* and hence had to be modelled separately.

For this purpose, the external torque is fed as a signal into the modelled Hirth clutch and converted into a force via equation 4.16. The effective radius is hereby calculated dynamically depending on the height with which the teeth overlap. For the jerking force, equation 4.12 was implemented into the simulation.

The calculated forces are then added together and translated via an *Ideal Force Source* into the mechanical force, which then acts on the shifting shaft. The resulting combination on the Simulink canvas, can be seen in Figure 4.7. The input $T$ is for the torque, applied on the output. $M$ is an output for the current mode, where 0 is disengaged and 1 is engaged. The mechanical translation port is $S$ for the shifting shaft. And the mechanical rotations ports $B$ and $F$ are the base and the follower.

Since the gear consists of two Hirth clutches, two clutches were implemented. The follower $F$ of each clutch is connected to the shifting shaft and the base $B$ to either the sun or the carrier. Through a translational movement of the shifting shaft, either one of the clutches is supposed engage. The next section will focus on how this movement was implemented.

Before that, the implementation of the springs is discussed. In order to reduce the impact when engaging the clutch, and thus the load on the teeth, two springs are integrated into the gear. These allow the Hirth serration on

the shifting shaft to move axially relative to the shaft. In the engaged state, the springs are compressed to such an extent that the Hirth serration can no longer move relative to the shifting shaft. To implement this concept in the Simulink model, a combination of three elements is required, which are connected in parallel:

- the actual *Translational Spring* with a constant spring rate,
- a *Translational Hard Stop* which limits how far the Hirth serration is able to move on the shaft and
- a *Translational Friction* which prevents the Hirth serration from moving on the shaft without external forces.

The *Translational Hard Stop* assumes a spring-damping system for each end of the range of motion, which hugely increases the complexity behind the simulation. However, without the *Translational Hard Stop* an indefinite movement of the Hirth gearing would be possible, which is not purposeful.

Furthermore, the built-in *Translational Springs* have the disadvantage that they only act on the translational Simscape domain. However, as can be seen in Section 4.3.1, the two domains translation and rotation also act on each other due to the inclined teeth. Thus, the actual translational spring also affects the torsional stiffness of the teeth. Another idea for implementing the springs was therefore to take the springs into account in the settings of the *Hirth clutch*. For the calculation of the serration, a stiffness of the teeth must be specified. This stiffness can be adjusted to include the separately installed spring, as shown in the following chapter. Because of the complexity of the first variant, the behaviour of the simulation is harder to understand. Thus, the second variant was chosen for the implementation of the springs.

### 4.3.4 Parameters of Simulated Hirth Clutch

The axial and rotational spring forces of the teeth are modelled similar to the forces in Figure 4.6. For simplicity, it is focused only on the stiffness and the damping is neglected. The spring force in normal direction is divided into an axial and a rotational force. Each force is calculated with $F_{c_i} = c_i \cdot x_i$, where $F_{c_i}$ is the spring force, $c_i$ the stiffness in the according direction and $x_i$ the displacement. With the adaptation of the force triangle

$$F_N = c_N \cdot x_N = c_A \cdot x_A + c_T \cdot x_T \tag{4.17}$$

applies, where N is the normal, A the axial and T the tangential direction. A division through $x_N$ and use of the trigonometric functions results in

$$c_N = \sin(\gamma) \cdot c_A + \cos(\gamma) \cdot c_T \tag{4.18}$$

where $\gamma$ is the half tooth flank angle. In Creo Simulate, a static finite element method simulation was used for the derivation. The result of this analysis was the normal stiffness of the teeth itself with 18000 N/mm for the sun and 30000 N/mm for the carrier.

For $\gamma = 45°$ this force is equally divided to $c_A = c_T = c_N/\sqrt{2}$. For the axial stiffness, the actual spring on the shaft is in line with the axial stiffness. This leads to the updated stiffness of

$$c_{N,new} = \frac{\sqrt{2}}{2} \cdot \left( \frac{1}{c_{spring}^{-1} + \sqrt{2} \cdot c_N^{-1}} + \frac{c_N}{\sqrt{2}} \right) \tag{4.19}$$

where $c_{spring}$ is the stiffness of the spring installed on the shifting shaft. For $c_{spring} = 10$ N/mm, the normal stiffness for sun is 9000 N/mm and for the carrier 15000 N/mm.

With this the settings of the Hirth serration were set as displayed in Table 4.1. The kinetic friction torque of the *Logic-Controlled Clutch* was set to 5 Nm, since it is assumed that the axial force is high enough to keep the Hirth teeth engaged.

**Table 4.1:** Relevant settings for simulation of the Hirth serration

| Name | Value for sun | Value for carrier |
|---|---|---|
| Effective radius | 16.25 mm | 22.5 mm |
| Normal stiffness | 9000 N/mm | 15000 N/mm |
| Kinetic friction torque | 5 Nm | 5 Nm |
| Tooth height | 1.2 mm | 1.85 mm |
| Clearance to idle | 0.7 mm | 0.65 mm |
| Sliding friction coefficient | 0.11 | 0.11 |

## 4.4 Movement of the Shifting Shaft

The movement of the shifting shaft was a challenge, as the actual mechanism for this has not yet been developed. Furthermore, neither the exact parameters nor the regulation are specified. Thus, only the mechanical result can be modelled and even that only roughly. Again, there are several solutions.

First, a physical translation in Simscape can be given into the system either by an *Ideal Force Source* or an *Ideal Translational Velocity Source*. Both variants have been tried and are briefly evaluated here. A first idea was to use an *Ideal Force Source* in combination with a position control. However, it was difficult to find a controller that would move the shifting shaft in the right velocity and still react quickly enough to the impact of the clutch engagement. As an alternative, without control, only a small force was applied to move the shifting shaft and full power only when the clutch is engaging. However, this resulted in a problem with another *Ideal Force Source*, which is used to apply the axial transmission force on the shifting shaft. It is problematic since two *Ideal Forces* act on each other.

After excluding these two possibilities, it was assumed that the movement of the shifting shaft is so well controlled by the mechanism developed later that it can properly follow a target trajectory despite the occurring forces. With this assumption, it was possible to mathematically calculate a trajectory that moves the shifting shaft so that it stops exactly at the end points. The velocity required for this was converted into a mechanical translation via an *Ideal Translational Velocity Source* and applied to the shifting shaft. The user of the simulation specifies a maximum velocity and maximum acceleration that the shifting shaft can reach. The disadvantage of this method is that no matter how high the force applied on the shifting shaft, it has exactly the given ideal velocity. Therefore, the force that the shifting shaft must deliver to reach this trajectory is only measured and reported to the user. The user must then evaluate whether the force to be applied can be realised by the drive or not.

The code for calculating the trajectory can be opened within the simulation. The associated flow chart can be seen in Figure 4.8. Roughly explained, it is checked at a certain frequency whether an immediate braking leads to a halt of the shifting shaft at the correct position. If this is the case, the shaft is maximally braked. If this is not the case, it is either accelerated to the maximum or, if the maximum velocity has already been reached, the maximum velocity is maintained. The frequency of this process was set to 1000 Hz, as this is the sampling rate of the input data.

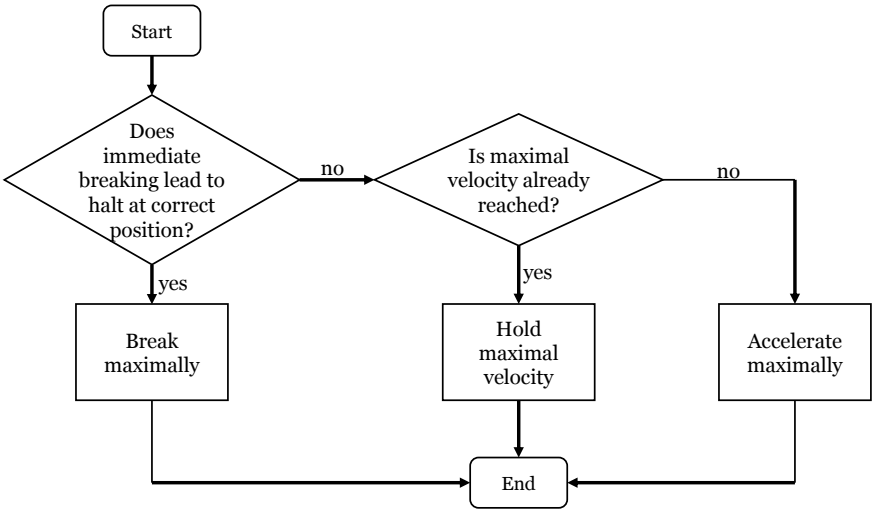


**Figure 4.8:** Flow chart of trajectory calculation

## 4.5 Derivation of Input Data

Four different input data are required, which will be discussed in this chapter. A distinction is made between data that results from the chosen application of the gear and data for the basis of the shifting actuator.

### 4.5.1 Data of Application

In Chapter 2.2 the chosen application was already explained and the required data discussed. The specific data of Figure 2.3 had to be digitised manually. For this, data points were read of the plots and a curve was created using the Matlab function *spline*. To get the angular velocity out of the angle, the spline for the angle was derived. As a result, the maximum angular velocities can be determined to 160 —°/s in stance and 370 °/s in swing phase. For the torque, the weight of TORO was used for de-normalizing, which is 76.4 kg [Eng+14]. This means that the maximum absolute torque is 122.24 Nm in stance or 38.2 Nm in swing phase. Since commercially available servo motors can only generate significantly lower torques, but offer higher speeds than required, a harmonic drive gear with a ratio of 30:1 is assumed to be installed in the drive line behind the switch-able gear. This increases the required rotational speed of the motor by a factor of 30, but at the same

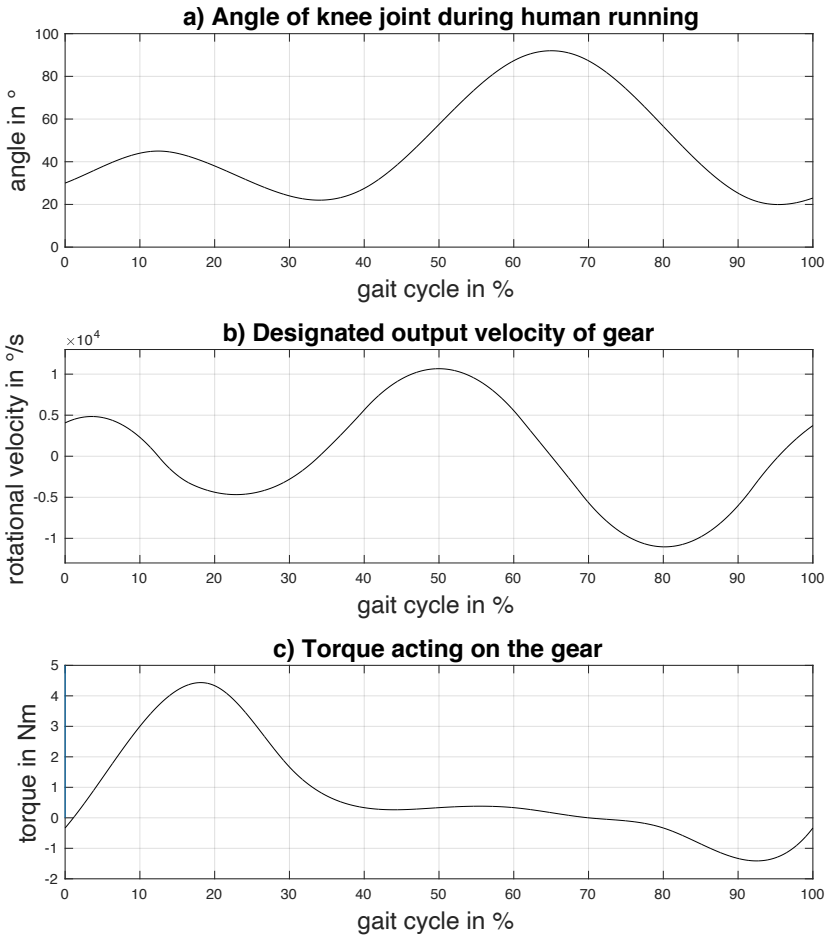


**Figure 4.9:** Input plots for simulation: a) angle of joint, b) angular velocity and c) torque to be applied. Respectively for the knee joint and plotted over the course of one gait cycle. Derived plots from [Nov98]

time only $30^{-1}$ of the torque acts on the motor. With these conversions, the plots in Figure 4.9 were created.

From this data, the input plots were derived. At the beginning of the simulation, the shifting shaft first moves to gear 1 before the angular rotation properly starts. Therefore, the input data was adjusted using a Matlab script. The input shaft rotates only slowly for this transition phase to prevent a direct encounter of the teeth of both clutch halves. At the same time, no

torque is applied to the output during this transition. After the run-in phase, the gear cycle is run through twice for both the angular velocity and the torque. The data are stored in two MAT-files, which are later loaded into the simulation.

The gear selection is carried out manually beforehand and is also integrated in the Matlab script. By analysing the course of angular velocity and torque, the shifting points were determined manually and then iteratively optimised using the gear simulation. The optimisation was started at points with a small possible torque and a relatively low velocity (both in absolute value). The final shifting values within one gait cycle are at 32.5% from gear 1 to 2 and at 94.4% the other way around. By determining the shifting times, a plot is created, which in turn is saved in another MAT-file and later loaded into the simulation.

### 4.5.2 Data for the Shifting Actuator

The maximum speed and maximum acceleration of the shifting shaft, which depend on the mechanism used, are specified in the dataflow "Boundaries of shifting actuator". In order to obtain approximate values, calculations were carried out for the examples in Chapter 2.3. Besides these two, the maximum apply-able force is required for later comparison with the results.

#### 4.5.2.1 Calculations for Lead Screw Mechanism

For the lead crew mechanism, the possible output force $F_{max}$ resulting from the maximum motor torque $\tau_{max}$ is calculated according to [SDP14, p. 51] as

$$F_{max} = \tau_{max} \cdot \frac{2}{d_S \cdot \tan(\varphi + \rho)} \cdot \eta \tag{4.20}$$

$$\text{with } \varphi = \arctan(\frac{p_h}{d_S \cdot \pi}), \tag{4.21}$$

where $d_S$ is the pitch diameter of the screw, $\varphi$ the pitch angle, $\rho$ the sliding friction angle, $p_h$ the lead pitch and $\eta$ the efficiency. For the maximum velocity $v_{max}$, the lead pitch per turn is required. The calculation is

$$v_{max} = \omega_M \cdot \frac{p_h}{2\pi}, \tag{4.22}$$

where $\omega_M$ is the angular velocity of the motor. Specifically for new switchable gear, the maximum acceleration is calculated via the torque equilibrium

$$\tau_{nom} - \tau_{mass} - \tau_{inertia} = 0, \tag{4.23}$$

where $\tau_{nom}$ is the nominal motor torque, $\tau_{mass}$ the torque resulting from the mass to be translationally moved and $\tau_{intertia}$ the torque resulting from the inertia to be rotationally moved. They are calculated via

$$\tau_{mass} = (m_{lead} + m_s) \cdot \ddot{x}_A \cdot \frac{d_S}{2} \cdot \tan(\varphi + \rho) \cdot \eta \text{ and} \tag{4.24}$$

$$\tau_{inertia} = (I_M + I_{lead}) \cdot \alpha_{lead} = (I_M + I_{lead}) \cdot \frac{\ddot{x}_A \cdot 2\pi}{p_h}, \tag{4.25}$$

where $m_{lead}$ is the mass of the lead screw, $m_s$ of the shifting shaft, $\ddot{x}_A$ its acceleration, $I_M$ the inertia of the motor, $I_{lead}$ of the lead screw and $\alpha_{lead}$ its angular acceleration. With 4.24 and 4.25 inserted in 4.23, $\ddot{x}_A$ is

$$\ddot{x}_A = \tau_{nom} \left( (m_{lead} + m_s) \frac{d_s}{2} tan(\varphi + \rho)\eta + (I_M + I_{lead}) \frac{2\pi}{p_h} \right)^{-1}. \tag{4.26}$$

For the lead screw mechanism the motor, which the calculation is based on, is the RoboDrive motor ILM-70x18 [TQS], which is widely used within the DLR and has a geometry, which fits the requirements. For the geometry of the lead screw, the assumptions in Table 4.2 were made. Hereby one turn of the motor results in the required displacement of 4 mm.

With this the maximum force $F_{max}$, maximum velocity $v_{max}$ and maximum acceleration $a_{max}$ for the simulation were calculated according to equations 4.20, 4.22 and 4.26 to

$$F_{max} = 182.8\,\mathrm{N}, \tag{4.27}$$

$$v_{max} = 22.49\,\mathrm{mm/s} \text{ and} \tag{4.28}$$

$$a_{max} = 6.195 \cdot 10^3\,\mathrm{mm/s^2}. \tag{4.29}$$

**Table 4.2:** Assumed values for calculation of lead screw mechanism

| Name | Formula | Value |
|---|---|---|
| Maximum motor torque | $\tau_{max}$ | 4.05 N m |
| Nominal motor torque | $\tau_{nom}$ | 1.24 N m |
| Angular velocity of the motor | $\omega_M$ | 2120 rpm |
| Inertia of the motor | $I_M$ | 0.321 kg cm$^2$ |
| Mass of the shifting shaft | $m_s$ | 400 g |
| Mass of the lead screw | $m_{lead}$ | 300 g |
| Inertia of the lead screw | $I_{lead}$ | 0.9375 kg cm$^2$ |
| Pitch diameter | $d_s$ | 60 mm |
| Lead pitch | $p_h$ | 4 mm |
| Pitch angle | $\varphi$ | 1.459° |
| Sliding friction angle | $\rho$ | 15° |
| Efficiency | $\eta$ | 0.4 |

#### 4.5.2.2 Calculations for Cam Mechanism

The calculation for both cam mechanisms are the same and hence summarised in this chapter. For the calculation of the output force $F_{out}$, the power is assumed to be

$$P_{out} = \eta \cdot P_{in}, \tag{4.30}$$

where $P_{out}$ is the output power, $\eta$ the efficiency and $P_{in}$ the input power. Since the cam mechanism has less friction than the lead screw, a slightly higher efficiency of 0.5 is assumed here. For a rotation at the input and a translation at the output, the following applies:

$$F_{out} \cdot v_{out} = 0.5 \cdot \tau_{in} \cdot \omega_{in} \tag{4.31}$$

where $v_{out} = \dot{x}_A$ is the translational velocity which results from the motor torque $\tau_{in}$ and motor angular velocity $\omega_{in} = \omega_M$. It follows for the maximum transmittable force $F_{max}$

$$F_{max} = 0.5 \cdot \tau_{max} \cdot (\frac{\omega_M}{\dot{x}_A})_{max} \tag{4.32}$$

where $\tau_{max}$ is the maximum torque of the motor. The value $\omega_M/\dot{x}_A$ is dependent on the geometry and the shifting time.

For the cam mechanism, the ILM70x18 is used as well. A Matlab script was created for the detailed calculation of the rather complex trajectory. The complete calculation for one example geometry can hence be found in Appendix C.1. The variables used in this special example are shown in table 4.3. For equal force distribution it is assumed that two rollers are used, so that the displacement of 4 mm must be achieved by a half turn of the motor. The results of the calculation for the cam mechanism are

$$F_{max} = 530.1\,\mathrm{N}, \tag{4.33}$$

$$v_{max} = 45.00\,\mathrm{mm/s} \text{ and} \tag{4.34}$$

$$a_{max} = 788.2\,\mathrm{mm/s^2}. \tag{4.35}$$

**Table 4.3:** Assumed values for calculation of a cam mechanism

| Name | Formula | Value |
|---|---|---|
| Maximum motor torque | $\tau_{max}$ | 4.05 N m |
| Nominal motor torque | $\tau_{nom}$ | 1.24 N m |
| Angular velocity of the motor | $\omega_M$ | 2120 rpm |
| Mass of the shifting shaft | $m_s$ | 400 g |
| Target displacement | $x_{max}$ | 4 mm |
| Shifting time | $t_s$ | 0.1 s |

#### 4.5.2.3 Calculations for Snapping Mechanism

For the snapping mechanism, only the snapping is evaluated here. The mechanism to tension the spring is not considered.

The calculation of shifting shaft's trajectory in the simulation does not work in this case due to the different dynamics. While a motor would brake towards the end, the spring only stops when it hits the end. This behaviour could not be realised with the trajectory neither was it possible to develop another shifting solution. Hence to simulate the key characteristics of the snapping mechanism, the goal was to move the shifting shaft rather quickly as one would expect from the release of a tensioned spring.

To calculate the acceleration a rather short shifting time is assumed. The approximate acceleration is then calculated via the equation

$$\ddot{x}_A = \frac{\Delta \dot{x}_A}{\Delta t_s} = \frac{\Delta x_A}{(\Delta t_s)^2}, \tag{4.36}$$

where $\ddot{x}_A$ is the acceleration of the shifting shaft, $\dot{x}_A$ its velocity, $x_A$ its displacement and $t_s$ the time needed for shifting. To realise a fast movement, there is no maximum velocity given. The input of the simulation therefore is $v_{max} = 10^5\,\mathrm{mm/s}$, which can not be reaches within the shifting time.

Since the force of the spring decreases in the course of the shifting process, not the largest force is taken as the critical maximum force, but the pre-tensioning force, that still is applied when the clutch is coupled-in. It is calculated with

$$F_{max} = x_{s0} \cdot c_{spring}, \tag{4.37}$$

where $x_{s0}$ is the pre-tensioned displacement of the spring.

With the assumed values in Table 4.4 the inputs for the simulation are

$$F_{max} = 300\,\mathrm{N}, \tag{4.38}$$

$$v_{max} = 10^3\,\mathrm{mm/s} \text{ and} \tag{4.39}$$

$$a_{max} = 8.444 \cdot 10^3\,\mathrm{mm/s^2}. \tag{4.40}$$

| Name | Formula | Value |
|---|---|---|
| Spring rate | $c_{spring}$ | $30\,\mathrm{N/mm}$ |
| Mass of shifting shaft | $m_s$ | $400\,\mathrm{g}$ |
| Minimum displacement (sun) | $x_A$ | $1.9\,\mathrm{mm}$ |
| Pre-tensioned displacement | $x_{s0}$ | $10\,\mathrm{mm}$ |
| Shifting time | $t_s$ | $0.015\,\mathrm{s}$ |

**Table 4.4:** Assumed values for calculation of a snapping mechanism

# 5 Validation

In the following, the validity of the simulation is shown. First, a look is taken at one example output with suitable input variables. Then, with changing the inputs, different physical situations are simulated and the output of the simulation is compared to the expected behaviour of the gear. For this chapter, only two of the outputs are considered: the position of the shifting shaft and the comparison of the measured to the targeted angular velocity.

The input data depending on the application is not varied. The maximum velocity of the shifting shaft is set to $v_{max} = 50\,\mathrm{mm/s}$ and the maximum acceleration to $a_{max} = 1000\,\mathrm{mm/s^2}$ and hence not set for a specific application. The resulting plot can be seen in Figure 5.1. For the measured velocity, the shifting point can clearly be seen. Since the shifting shaft is shortly without connection to the drive, the disturbing torque acting on the shifting shaft accelerates it. This results in peaks in the plot or a higher angular velocity difference when the clutches engage again.

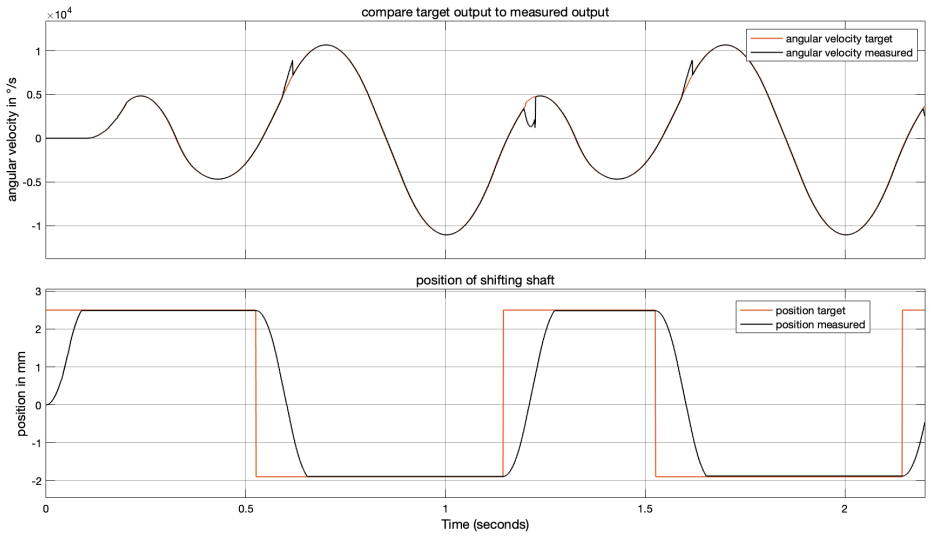


**Figure 5.1:** Output data for a functioning gear

## 5.1 Scenario One: Slow Movement of Shifting Shaft

Firstly, a too slow movement of the shifting shaft is tested. To enable this, both translational velocity and acceleration can be adjusted. The result in both cases is a slow translation were the end points can not be reached within the shifting period.

It was decided to assume a low velocity of 2 mm/s and a higher acceleration of 1000 $mm/s^2$. In Figure 5.2 can be seen, that the shifting shaft moves very slowly. As expected, the measured angular velocity is increased by the output when not coupled in. At t = 0.32 s, the clearance between the Hirth serration teeth is overcome and the teeth touch. The expectation here is that the serration on the shifting shaft is pushed backwards by the developed axial force and then moves forward again into the next tooth space. The angular velocity of the shaft is hereby supposed to slowly and choppily adjust to the input velocity (or targeted velocity). In the plot, the adjustment is not choppy, but nevertheless slow and thus reasonably well mapped. In the later course of the simulation, the selection of the gear changes faster and the Hirth serrations are not able to couple-in completely. The angular velocity reacts as expected and is only driven by the output torque.

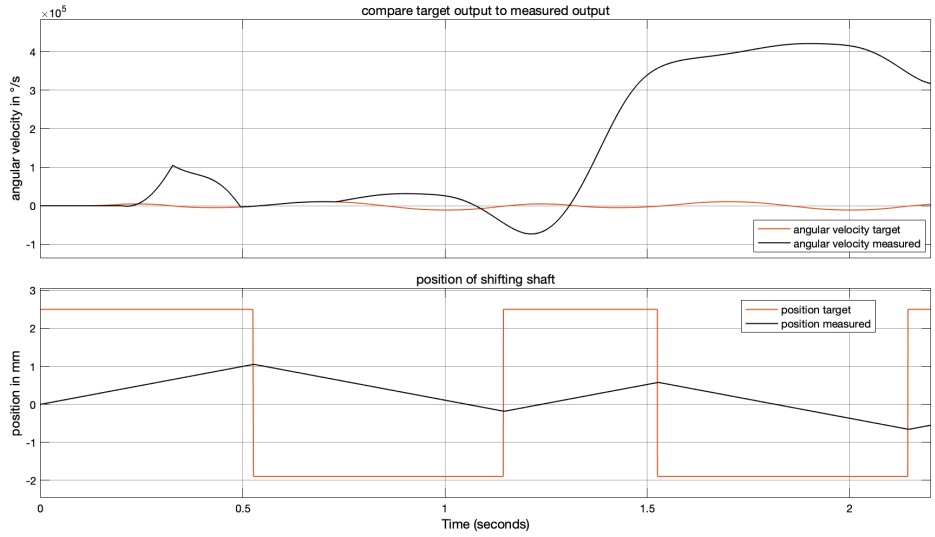


**Figure 5.2:** Output data for a too slow translation of the shifting shaft

## 5.2 Scenario Two: Fast Movement of Shifting Shaft

For a fast movement, again translational velocity and acceleration can be modified. For a moderate acceleration, a higher maximum velocity is often not reached (compare Figure 6.3). Hence, the focus here is on the higher acceleration. For a acceleration up to $1.17 \cdot 10^4\,\mathrm{mm/s^2}$, the measured movement of the shifting shaft is as expected and the simulation works. However, a higher acceleration causes the shifting shaft to move further than it would actually be physically able to. This can bis seen in Figure 5.3 for a maximum acceleration of $1.2{\cdot}10^4\,\mathrm{mm/s}$ and a maximum velocity of $500\,\mathrm{mm/s}$. The reason for this is the F2 function. Here the movement is calculated discretely with a sample time of $0.001\,\mathrm{s}$. In case of a too high acceleration, the function does not notices in time that the end of the range of motion has actually already been reached. However, in purely physical terms, an acceleration of this magnitude is difficult, if not impossible, to achieve for the drive. Therefore, it is acceptable that these cases can be excluded for the simulation.

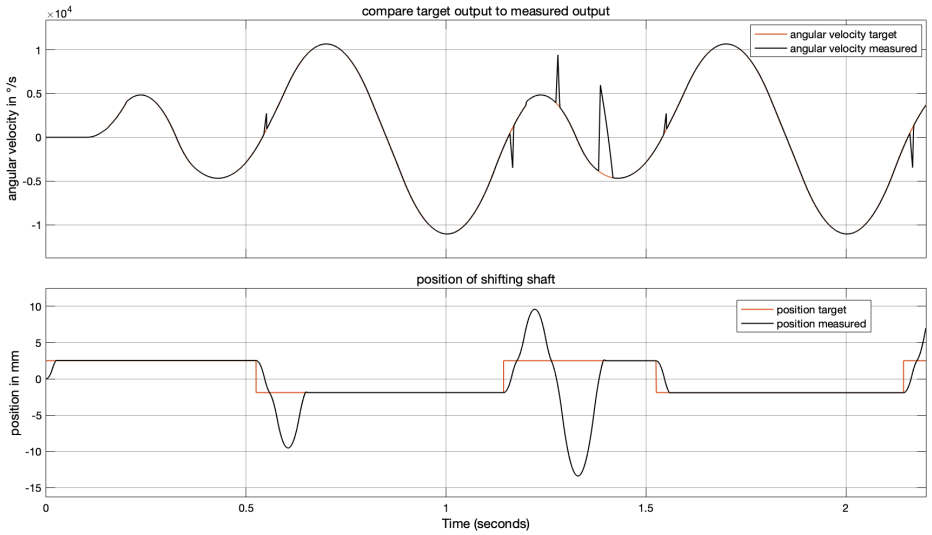


**Figure 5.3:** Output data for a too fast translation of the shifting shaft

## 5.3 Scenario Three: Decoupled Output Torque

If the output torque is decoupled from the gear and the shifting shaft is in idle mode, its rotation decreases very slowly, mainly due to friction. In Figure 5.4 it can be observed that as soon as the idle mode is reached, the angular velocity remains constant and thus moves away from the target curve. This is not the exact physical behaviour, but still within the limits.

When engaging the clutch, at 1.2 s a velocity peak can be seen. This is explained as follows: To reach the target angular velocity at the output, the input angular velocity must be four times as high in carrier mode (ratio 4:1). Accordingly, the input velocity has to be adjusted to the next gear during the coupling process. In the simulation, this is adjusted by the signal *Da.3*, flowing back to F3. Since this results in an algebraic loop, a delay must be integrated for interruption. This leads to the input velocity being adjusted too late and hence the output following the wrong velocity. As soon as torque is applied at the output, this problem is obscured and therefore negligible.

In summary, it can be said that there are smaller problems within the simulation, but these have a rather small influence. Hence, the simulation is considered valid.

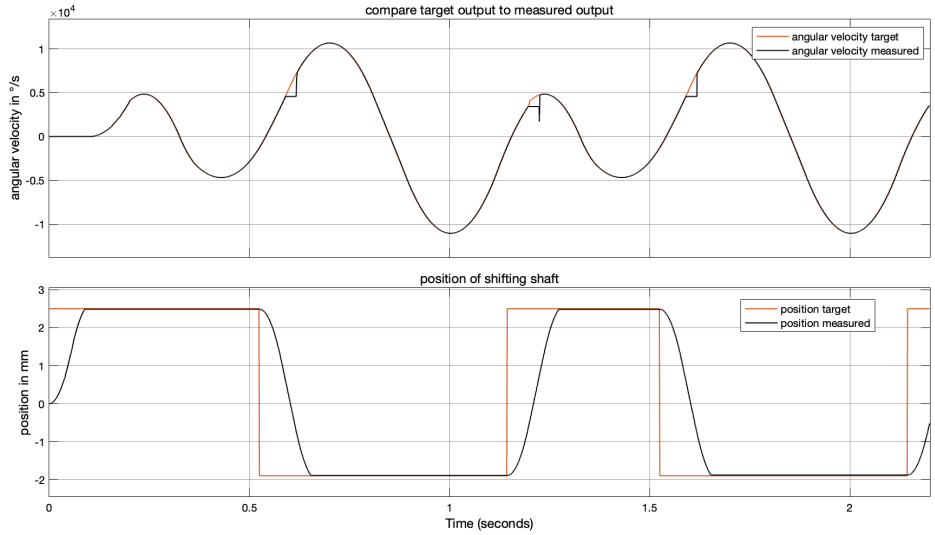


**Figure 5.4:** Output data for a decoupled output torque

# 6 Results

After the validation, the data from Chapter 4.5 was given into the simulation. The results are discussed in the following sections for each of the actuators. For each simulation run, four output plots are given.

The first plot shows both the target position and the measured position of the shifting shaft. The target position results directly from the gear that was selected at the input. The measured one shows were the shaft actually is. For a positive displacement, the associated clutch is the carrier one and for a negative displacement respectively the one of the sun.

Than the measured translational velocity with which the shifting shaft moves is plotted. The third window plots the force that acts on the shifting shaft. It is measured directly at the shaft and therefore displays the force resulting from both Hirth couplings.

Lastly to check the correct functioning of the gear, the angular velocity at the output-side is compared to the target angular velocity required to fulfil the application requirements. The target angular velocity consists of the run-in phase and following two runs of the gait cycle. Each cycle consists of two peaks. For the first and third positive peak, gear 1 is set. It is then shifted to the second gear for the second and forth peak.

## 6.1 Lead Screw Mechanism

For the lead screw, the adjustment of the measured position to the target is rather slow and a steady acceleration can be seen at the beginning and end of the shifting process. The shifting process is hereby the time where the two curves are separate from each other. The time required for this approximately is 0.196 s. In between, either one of the Hirth clutches is coupled-in.

Within the shifting process, the according velocity is first accelerated to its maximum. It stays there until it is braked to zero in the end. As soon as one of the clutches is reached, the shifting shaft has a velocity of 0.

The force shows two mayor characteristics. First there is a slowly developing force when either one of the clutches is coupled-in. This is the force that needs to be applied to keep the Hirth serrations from pushing themselves

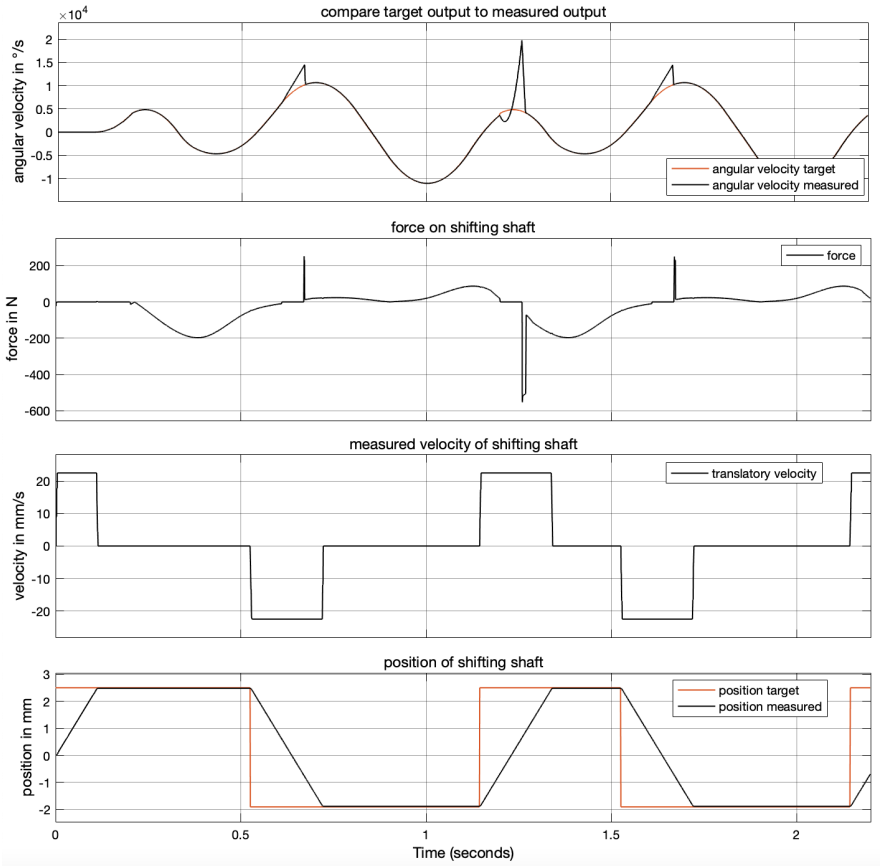


**Figure 6.1:** Output data for the lead mechanism

apart. It can be seen that independently of the angular direction the torque is applied, the resulting force is directed away from the Hirth serration. This means for the Hirth carrier a negative force and for the Hirth sun a positive force. The second mayor characteristic is the impact force of the in-coupling process. It develops as soon as the clearance between idle and the chosen gear is overcome. Again the direction points away from the Hirth serration. The height of the peaks is 260 N for the in-coupling of the sun and -570 N for the carrier. Shortly before those peaks, the occurring force is 0 when the idle gear is set. In the course of the plot, a few very small peaks can be seen, for example at 0.53 s and 0.72 s. They are associated with the force required to accelerate the shifting shaft into movement.

Lastly, a look is taken at the target and measured angular velocities. They are the same for most of the time and the only differences occur within the

shifting process. As explained in Chapter 5, the output torque accelerates the shifting shaft, which leads to the visible angular velocity peaks. For the first shifting process from carrier to sun, the torque acts in a positive angular direction. Hence the output is as well positively accelerated. For the shift between sun to carrier it is shifts in a moment where the torque changes from a negative to a positive direction. Hence the output shaft is first accelerated in a negative and following in a positive angular direction. Since the shifting happens rather slow, the peaks are rather high with a height of $\Delta\omega = 4200°/s$ for in-coupling of the sun and $\Delta\omega = 14750°/s$ for the carrier. High peaks show that the angular velocities move far apart, which increases the jerk on the teeth at contact.

## 6.2 Cam Mechanism

For the cam mechanism, the plots are in general similar to the ones of the lead screw. Even though the translational acceleration is lower than the one from the lead screw, a higher velocity can be reached. Hence, the position develops faster and the time for the shifting process decreases to 0.144 s. For the velocity, it can be seen that at the end of the shifting process there is a step where the acceleration is higher. This is due to an inaccuracy of the discrete trajectory calculation, which could not be resolved. The plot for the force is again very similar to the one of the lead screw. The slowly developing force while transmitting torque has the same amount, as was expected. Solely the peaks when coupling-in are higher. They are 210 N for the shifting process from carrier to sun gear and -540 N the other way.

Similar to the lead screw mechanism, the target and measured velocity match when either one of the clutches is coupled in. However, due to the shorter shifting time, the disturbance torque on the output side of the gear, has a smaller impact. The shorter time phase leads to a smaller acceleration due to the disturbing torque and an angular velocity increase of $\Delta\omega = 1700°/s$ for the sun-in-coupling and $\Delta\omega = 1900°/s$ for the carrier.

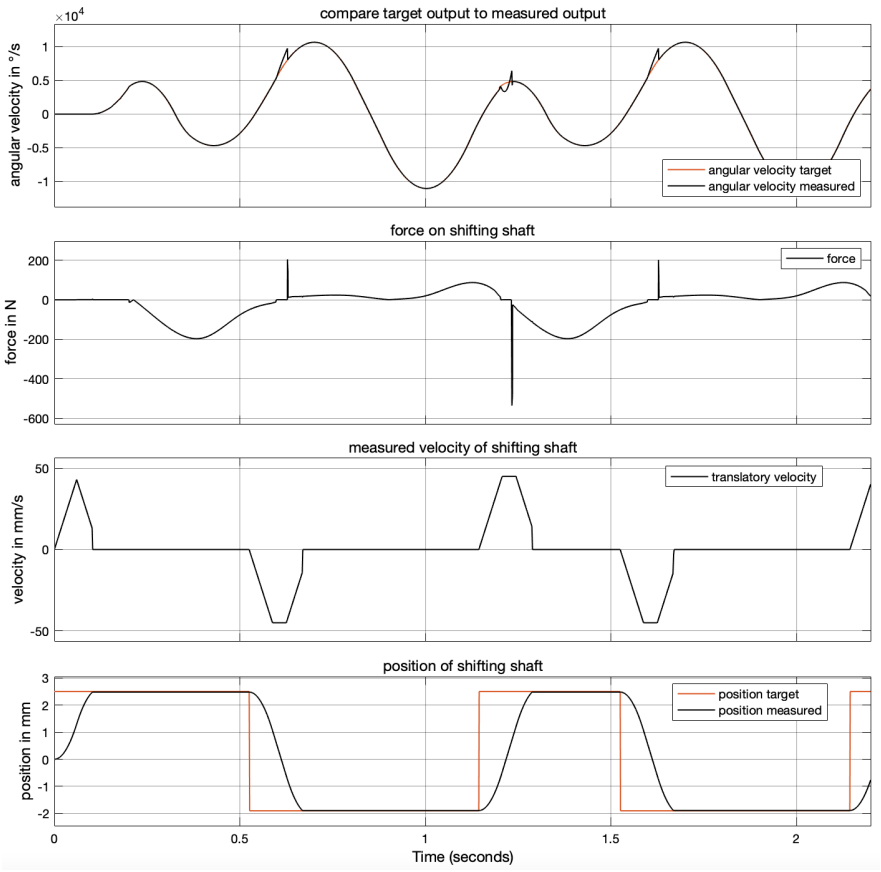


**Figure 6.2:** Output data for the cam mechanism

## 6.3 Snapping Mechanism

For the snapping mechanism, the trend continuous. The shifting time is only 0.054 s. Since this value changes the shifting behaviour, the shifting timing was again optimized. The shifting worked optimally for shifts at 39% and 99% of the gait cycle. With that, the plot for the force has its peaks at 195 N for the first shift and at -511 N for the second shift of each cycle. Since the shifting time is so much shorter, the peaks within the coupling process are smaller as well with a height of $\Delta\omega = 394°/s$ for the sun in-coupling and $\Delta\omega = 1594°/s$ for the carrier.

Even though the shifting process does not correspond to the actual movement, the resulting angular velocity plot is assumed to be accurate enough for a comparison.

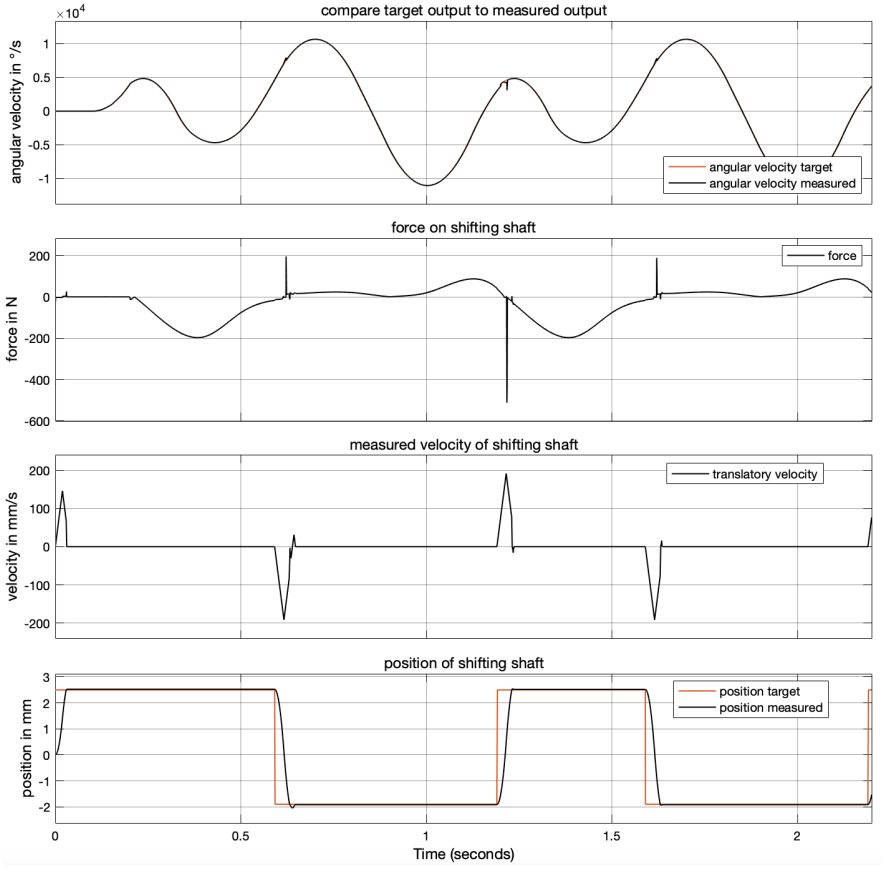


**Figure 6.3:** Output data for the snapping mechanism

## 6.4 Recommendation of One Shifting Variant

**Table 6.1:** Comparison of results from different shifting variants

| | Lead Screw | Cam | Snapping |
|---|---|---|---|
| Shifting time | 0.196 s | 0.144 s | 0.054 s |
| Required force | 260 N | 210 N | 195 N |
| | -570 N | -540 N | -511 N |
| Absolute, possible force | 182.8 N | 530.1 N | 300 N |
| Angular velocity peaks | 4200 °/s | 1700 °/s | 394 °/s |
| | 14750 °/s | 1900 °/s | 1594 °/s |

In Table 6.1 the received values of the simulation are compared. The main difference between the variants is the length of the shifting period and hence the height of the outbreak of the measured in contrast to the targeted angular velocity. For the lead screw mechanism, the shifting time is with 0.196 s the longest. For two shifts within one gait cycle of 1 s, nearly 40% of the time would be spent shifting gears and not actually transmitting torque. The lead screw mechanism is therefore not applicable.

Between one of the cams and the snapping mechanism, the latter is faster and hence the better choice. However, the actual construction of this unique approach is challenging, since not only the tensioning of the springs, but the securing of the shifting shaft while the spring is tensioned, needs to be integrated. Furthermore the movement of the shifting shaft was not accurately simulated for this case and has to be implemented to get at trustworthy result.

The second option, the cam mechanisms, are not yet the optimal choice. However, for the calculation of the trajectory, an easy approach was taken in this work. With an optimization of this trajectory, the cam might improve dramatically. This variant has the great advantage of a controlled movement. It enables an exact encounter of the teeth, since it is able to react even after the shifting process began. This is important since the angle with which the Hirth serrations meet, influences the force within the engagement process (compare equation 4.3). Furthermore the bearing of the moving elements is easier than for the snapping mechanism, since no jerky movements occur.

The cam mechanism is able to provide a force of 530.1 N. The required force is with 540 N only marginal higher and it is supposed that the optimisation of the trajectory also influences this values. Concerning the list of requirements

in Appendix A.1, it is able to fulfil all demanded points. Moreover, it fulfils many of the wishes, especially with the low shifting time of 0.144 s. In conclusion, an optimized cam mechanism is recommended. Between the two designs, the end cam is more compact than the cylindrical cam and therefore preferred according to the requirements in Appendix A.

## 6.5 Influence of Shifting Time

The most important note is that even within the same mechanism, the timing of shifting gears plays a great role. Figure 6.4 shows the peaks of angular velocity when shifting for three different timings. The input was set to $v_{max} = 50$ mm/s and $a_{max} = 1000$ mm/s$^2$, same as for the validation. The first scenario is the optimal shifting time that was optimized within the designing process. The second plot shows the outbreak of velocity for a similar, but not optimal timing (40% and 100% of gait cycle). It can be seen, that the outbreak of angular velocity as well as the shifting force is significantly higher. The third plot shows an outbreak of velocity when the shifting happens at a moment of higher torque (20% and 90% of gait cycle). It leads to a very quick acceleration that can not be caught again by the gears. A forth scenario would be shifting at a higher angular velocity difference (e.g. 50% and 80% of gait cycle). This leads to a higher stress on the teeth, which are thus worn down more quickly. However, this is not modelled within the simulation, but not recommendable to try.

The optimal shifting timing would be at a moment without load at the output side and a low relative angular velocity. For the perfect timing, the goal would be to shift in a way that the acceleration of the decoupled shifting shaft would be the same as the acceleration of the drive. This would lead to a rightfully accelerated shifting shaft even without motor contact. To modify this behaviour even further, the change in angular velocity could be calculated via the torque measured at the output. This makes it possible for the input shaft to be accelerated during shifting in such a way that both serration halves already have a very similar speed when engaging.

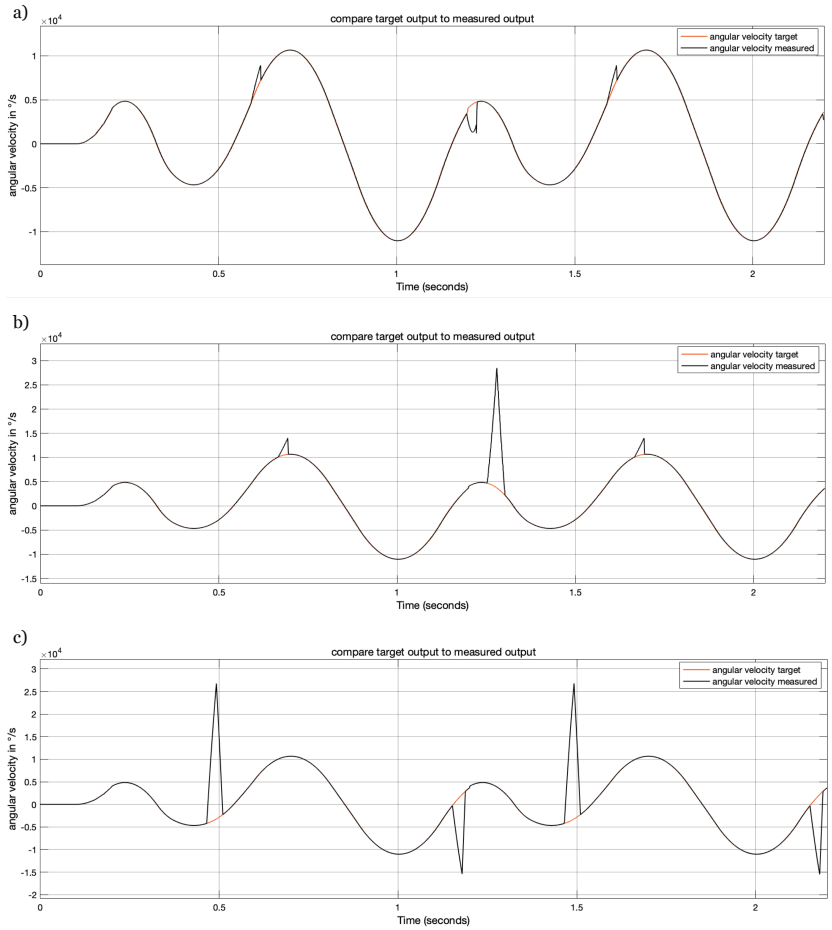


**Figure 6.4:** Measured angular velocity for inopportune switching

# 7 Summary and Future Work

As part of the designing process for the shifting actuator of a new switch-able gear, a comprehensive simulation of the shifting behaviour was developed in the course of this thesis. Restrictions had to be made for the simulation in order to guarantee feasibility in terms of time. Nevertheless, the simulation models the gear sufficiently well so that the results of the different actuators could be used to make a conclusive design recommendation for a cam mechanism.

Following this work, the modelling of the Hirth serration can be enhanced in order to obtain even better results for a future usage of the simulation. Furthermore, the translational motion of the shifting shaft is currently provided by an ideal trajectory, which is generally applicable, but does not model specific dynamics. This element can be replaced by the components of the selected actuator. This should be done especially for the snapping mechanism, as the trajectory does not model the actual dynamics well.

In order to optimise the switching behaviour, the influence of the angle at which the gears meet should also be investigated.

In conclusion, it can be said that the new switch-able gear is applicable for the knee joint of a humanoid running robot. Once the torque and angular velocity data have been specified for this biped, an analysis of the shifting timing can be performed and the designed mechanism can be tested.

# Appendix

# A Specifications of the Shifting Actuator

**Table A.1:** Specifications of translational actuator

| No. | D/W | Requirement | Specifications |
|---|---|---|---|
| 1 | | Geometry and dimensions | |
| 1.1 | D | outer shape | cylindrical |
| 1.2 | W | diameter | $\leq 77\,\mathrm{mm}$ |
| 1.3 | W | length | as short as possible |
| 1.4 | D | cylindrical hollow | $> 25\,\mathrm{mm}$ |
| 1.5 | W | cylindrical hollow | $\geq 35\,\mathrm{mm}$ |
| 2 | | Weight | |
| 2.1 | D | weight | $\leq 1000\,\mathrm{g}$ |
| 2.2 | W | weight | $\leq 200\,\mathrm{g}$ |
| 3 | | Kinetics | |
| 3.1 | D | translational displacement | $4 - 8\,\mathrm{mm}$ |
| 3.2 | D | shifting time | $< 500\,\mathrm{ms}$ |
| 3.3 | W | shifting time | $< 100\,\mathrm{ms}$ |
| 4 | | Manufacturing | |
| 4.1 | W | use of purchased parts | |
| 4.2 | W | costs | as low as possible |
| 5 | | Assembly and disassembly | |
| 5.1 | W | easy assembly | |
| 5.2 | W | disassembly possible | |
| 6 | | Usage | |
| 6.1 | D | field of application | without major restrictions |
| 6.2 | W | stability | high |
| 6.3 | W | durability | long |
| 6.4 | W | noise level | low |
| 6.5 | W | maintenance | easy |

D...demand, W...wish

# B Short User Guide for the Simulation

Two files are relevant for the use of the simulation. In the Matlab script *calc_plots.mlx* the plots for the inputs are calculated from the data set. Here, the shifting timing can be changed. The second file is the actual simulation *simulation.slx*. To be able to run the file, the Simulink version 2021a is needed as well as the extension Simscape with the library Simscape Driveline. In the simulation, the maximum speed and maximum acceleration can be adjusted inside the model workspace.

# C Further Calculations

## C.1 Derivation of the Values for a Specific Cam Mechanism

Calculation of the kinetics and kinematics of a barrel cam.

The following variables are time-dependent:

Angle : $\phi = \phi(t)\,;\ [\phi] = {}^{\circ}$
Angular velocity : $\omega = \omega(t)\,;\ [\omega] = \frac{^{\circ}}{s}$
Angular acceleration : $\alpha = \alpha(t)\,;\ [\alpha] = \frac{^{\circ}}{s^2}$
Axial displacement : $s = s(\phi(t))\,;\ [a] = \mathrm{mm}$
Axial velocity : $w = w(t)\,;\ [w] = \frac{\mathrm{mm}}{s}$
Axial acceleration : $a = a(t)\,; [a] = \frac{\mathrm{mm}}{s^2}$

Calculation of the translatory motion depending on angle:

$s(\phi) = a_0 + a_1\ \phi + a_2\ \phi^2\ + a_3\ \phi^3$
$v(\phi) = a_1 + 2a_2\ \phi + 3a_3\ \phi^2$

For the first part of the trajectory following conditions are given

$s(0) = 0$
$v(0) = 0$
$s\left(\frac{\phi_{\max}}{2}\right) = s_{\max}$
$v\left(\frac{\phi_{\max}}{2}\right) = 0.$

Hence it is given for the first part

$$s_1(\phi) = 12\ s_{\max}\Big(\tfrac{\phi}{\phi_{\max}}\Big)^2 - 16\Big(\tfrac{\phi}{\phi_{\max}}\Big)^3$$

and for the second part accordingly

$$s_2 = -12\ s_{\max}\Big(\tfrac{\phi}{\phi_{\max}} - \tfrac{1}{2}\Big)^2 + 16\Big(\tfrac{\phi}{\phi_{\max}} - \tfrac{1}{2}\Big)^3 + s_{\max}.$$

Since only one calculation needed for the derivation of the input data, the second part of the trajectory s2 is no longer considered. This equation derived after t is

$v(t) = \frac{d\, s(\phi(t))}{d\, t} = \frac{d\phi(t)}{d\, t} \frac{d\, s(\phi)}{d\phi}$
with $\frac{d\phi(t)}{\mathrm{dt}} = \omega\,(t)$
to $v_1(\phi) = \omega \left( \frac{24\,\phi\, s_{\max}}{{\phi_{\max}}^2} - \frac{48\,\phi^2\, s_{\max}}{{\phi_{\max}}^3} \right)$.

The second derivation similarly follows from

$a\,(\phi\,(t)) = \frac{d\,\omega(t)}{d\, t} * v\,(\phi\,(t)) + \omega\,(t) * \frac{d\, v(\phi(t))}{d\, t}$
to $a_1(\phi) = \left( \frac{24\, s_{\max}}{{\phi_{\max}}^2} - \frac{96\,\phi\, s_{\max}}{{\phi_{\max}}^3} \right) \omega^2 + \alpha \left( \frac{24\,\phi\, s_{\max}}{{\phi_{\max}}^2} - \frac{48\,\phi^2\, s_{\max}}{{\phi_{\max}}^3} \right) \omega$.

The time dependency is described by an cubic trajectory with the following boundary values:

$t_0 = 0$
$t_1 = t_s$
$\phi_0 = 0$
$\phi_1 = \frac{\phi_{\max}}{2} = 90°$
$\omega_0 = 0$
$\omega_1 = 0$

This leads to

$\phi(t) = 3 \cdot \phi_{max}/2 \cdot (t/t_s)^2 - 2 \cdot \phi_{max}/2 \cdot (t/t_s)^3$,
$\phi(t) = \frac{270\, t^2}{{t_s}^2} - \frac{180\, t^3}{{t_s}^3}$,
$\omega(t) = \frac{540\, t}{{t_s}^2} - \frac{540\, t^2}{{t_s}^3}$ and
$\alpha(t) = \frac{540}{{t_s}^2} - \frac{1080\, t}{{t_s}^3}$.

It is now focused on the first shifting process (from s=0 mm to s=4 mm). The following applies:

$\phi = \phi\,(t)$
$\phi_{\max} = 180°$
$s_{\max} = 4\mathrm{mm}$
$t_s = 0.1s$

Firstly, the angular variables are calculated to

$\phi(t) = 6750\,t^2 - 22500\,t^3$,
$\omega(t) = 13500\,t - 67500\,t^2$ and
$\alpha(t) = 13500 - 135000\,t$.

They are then inserted in the axial values, which results in

$$s_1(t) = 48\left(\frac{75\,t^2}{2} - 125\,t^3\right)^2 - 64\left(\frac{75\,t^2}{2} - 125\,t^3\right)^3,$$

$$v_1(t) = 96\left(75\,t - 375\,t^2\right)\left(\frac{75\,t^2}{2} - 125\,t^3\right) - 192\left(75\,t - 375\,t^2\right)\left(\frac{75\,t^2}{2} - 125\,t^3\right)^2$$

and

$$a_1(t) = 92\left(750\,t - 75\right){\sigma_1}^2 - 96\left(750\,t - 75\right)\sigma_1 + 96\left(75\,t - 375\,t^2\right)^2 - 384\left(75\,t - 375\,t^2\right)^2\sigma_1$$

where

$\sigma_1 = \frac{75\,t^2}{2} - 125\,t^3$.

The maximum values can be calculated from the formulas to

$a_{max} = 788.22\frac{mm}{s^2}$.
$v_{max} = 45.0\frac{mm}{s}$
$\alpha_{max} = 13500.0\frac{\overset{\circ}{}}{s^2}$
$\omega_{max} = 675.0\frac{\overset{\circ}{}}{s}$

The force is calculated according to equation 4.32 with

$$F_{max} = 0.5\;T_{\mathrm{maxMotor}}\left(\frac{\omega}{v}\right)_{\max} \;=\; 0.5\;T_{\mathrm{maxMotor}}\frac{\omega_{\max}}{v_{\max}}$$

$$[F] = N; [T] = \mathrm{Nm}; [\omega_{\max}] = \frac{\mathrm{rad}}{s}; [v_{\max}] = \frac{\mathrm{mm}}{s}$$

An example motor (RoboDrive ILM-70x18) has the following data:

$T_{Mmax} = 4.05\,\mathrm{Nm}$
$T_{Mnom} = 1.24\,\mathrm{Nm}$
$\omega_M = 2120\,\mathrm{rpm}$

It can be seen that the maximum angular-velocity while switching can be provided by the motor, since the possible angular velocity $\omega_{Mmax}$ is greater than the needed angular velocity $\omega_{Mmax}\omega_{max}$. The maximum applicable force while switching is calculated

$$F_{max} = 0.5 * T_{Mmax} * \omega_{max}/v_{max} * (1000 * \pi)/(180)$$
$$F_{max} = 530.1N$$

This values of course have to be re-calculated for the final switching mechanism. The values are only supposed to give a rough direction indication of the order of magnitude.

# References


[Bec+20] Stefan Beck, Uwe Griesmeier, Matthias Horn, Johannes Kaltenbach, Fabian Kutter, Thomas Martin, and Peter Ziemer. "Schaltbares Planetengetriebe". DE102019205748A1. Oct. 29, 2020 (cit. on p. 2).

[Bek+92] George A Bekey, J Kim Joung-woo, JoAnne K Gronley, Ernest L Bontrager, and Jacquelin Perry. "GAIT-ER-AID: An expert system for diagnosis of human gait". In: *Artificial Intelligence in Medicine* 4.4 (1992), pp. 293–308 (cit. on p. 8).

[Bók+10] G Bóka, L Lovas, J Márialigeti, and B Trencséni. "Engagement capability of face-dog clutches on heavy duty automated mechanical transmissions with transmission brake". In: *Proceedings of the Institution of Mechanical Engineers, Part D: Journal of Automobile Engineering* 224.9 (2010), pp. 1125–1139 (cit. on p. 6).

[DLR] DLR. *TORO*. URL: `https://www.dlr.de/rm/toro` (visited on 07/16/2021) (cit. on p. 7).

[Dua14] Chengwu Duan. "Analytical study of a dog clutch in automatic transmission application". In: *SAE International Journal of Passenger Cars-Mechanical Systems* 7.2014-01-1775 (2014), pp. 1155–1162 (cit. on pp. 6, 24).

[Dyn] Boston Dynamics. *Atlas*. URL: `https://www.bostondynamics.com/atlas` (visited on 08/16/2021) (cit. on p. 7).

[Eng+14] Johannes Englsberger, Alexander Werner, Christian Ott, Bernd Henze, Maximo A. Roa, Gianluca Garofalo, Robert Burger, Alexander Beyer, Oliver Eiberger, Korbinian Schmid, and Alin Albu-Schäffer. "Overview of the torque-controlled humanoid robot TORO". In: *2014 IEEE-RAS International Conference on Humanoid Robots*. 2014, pp. 916–923. DOI: `10.1109/HUMANOIDS.2014.7041473` (cit. on p. 32).

[Eno11] Staffan Enocksson. *Modeling in MathWorks Simscapeby building a model of an automatic gearbox*. 2011 (cit. on p. 6).

[Hab18] Horst Haberhauer. *Maschinenelemente*. Springer, 2018. Chap. Elemente der drehenden Bewegung. ISBN: 978-3-662-53047-4 (cit. on p. 6).

[Hir+98] Kazuo Hirai, Masato Hirose, Yuji Haikawa, and Toru Takenaka. "The development of Honda humanoid robot". In: *Proceedings. 1998 IEEE International Conference on Robotics and Automation (Cat. No. 98CH36146)*. Vol. 2. IEEE. 1998, pp. 1321–1326 (cit. on p. 7).

[Jah] Jahobr. *Umlaufrädergetriebe*. URL: `https://de.wikipedia.org/wiki/Umlaufr%C3%A4dergetriebe` (visited on 06/06/2021) (cit. on p. 2).

[Jia+11] Ming Jiang, Wei Chen, Yunqing Zhang, and Liping Chen. *Multi-domain modeling and simulation of AMT based on Modelica*. Tech. rep. SAE Technical Paper, 2011 (cit. on p. 6).

[Kai93] Heinz Kaiser. "Exzenterpresse oder Stanze mit schaltbarem Planetengetriebe". DE4309785C2. Mar. 25, 1993 (cit. on p. 2).

[Kal+18] Eberhard Kallenbach, Rüdiger Eick, Tom Ströhla, Karsten Feindt, Matthias Kallenbach, and Oliver Radler. *Elektromagnete: Grundlagen, Berechnung, Entwurf und Anwendung*. Springer-Verlag, 2018 (cit. on p. 13).

[Lin18] Heinz Linke. *Konstruktionselemente des Maschinenbaus 2*. Ed. by Bernd Sauer. Springer Berlin Heidelberg, 2018. Chap. Zahnräder und Zahnradgetriebe. DOI: `10.1007/978-3-642-39503-1` (cit. on pp. 6, 13).

[Loe+16] Florian Loeffl, Alexander Werner, Dominic Lakatos, Jens Reinecke, Sebastian Wolf, Robert Burger, Thomas Gumpert, Florian Schmidt, Christian Ott, Markus Grebenstein, et al. "The dlr c-runner: Concept, design and experiments". In: *2016 IEEE-RAS 16th International Conference on Humanoid Robots (Humanoids)*. IEEE. 2016, pp. 758–765 (cit. on p. 7).

[LTZ07] Jing Liu, Min Tan, and Xiaoguang Zhao. “Legged robots — an overview”. In: *Transactions of the Institute of Measurement and Control* 29.2 (2007), pp. 185–202. DOI: 10.1007/978-3-322-89521-9_13 (cit. on p. 7).

[Mat] Inc. MathWorks. *Making Optimal Solver Choices for Physical Simulation*. URL: https://de.mathworks.com/help/physmod/simscape/ug/making-optimal-solver-choices-for-physical-simulation.html (visited on 07/10/2021) (cit. on p. 20).

[Nov98] Tom F Novacheck. “The biomechanics of running”. In: *Gait & posture* 7.1 (1998), pp. 77–95 (cit. on pp. 8, 9, 33).

[OSE97] Martin Otter, Clemens Schlegel, and Hilding Elmqvist. “Modeling and realtime simulation of an automatic gearbox using Modelica”. In: *Proceedings of ESS*. Vol. 97. Citeseer. 1997, pp. 19–23 (cit. on p. 6).

[Per92] Jacquelin Perry. *Gait analysis : normal and pathological function*. Thorofare, NJ: SLACK, 1992. Chap. Normal Gait. ISBN: 9781556421921 (cit. on p. 8).

[Pez+05] Eugenio Pezzuti, Alessio Ubertini, Pier Paolo Valentini, and Leonardo Vita. “An integrated tool for design, shape modelling and performance analysis of 3D cam”. In: *International journal of computer applications in technology* 23.2-4 (2005), pp. 185–191 (cit. on p. 12).

[Pie08] Wolf Dieter Pietruszka. *MATLAB und Simulink in der Ingenieurpraxis: Modellbildung, Berechnung und Simulation*. Springer-Verlag, 2008 (cit. on pp. 6, 20).

[Rüt] AG Antriebe Rüthi. *Voith Hirth-Stirnverzahnung, Normringe und Zahnringe*. URL: https://antriebe.ch/admin/resources/voith-hirth-stirnverzahnung-normringe-und-zahnringe-2.pdf (visited on 08/16/2021) (cit. on p. 27).

[Sch18] Ewald Schmitz. “Lageranordnung und Planetengetriebe”. DE102016221958A1. May 9, 2018 (cit. on p. 2).

[SDP14] Philipp Schmalzhaf, Ruben Disterheft, and Gerhard Pfeil. *Grundlagen linearer Antriebstechnik*. Springer, 2014. DOI: 10.1007/978-3-658-03149-7 (cit. on pp. 10, 11, 34).

[TQS] GmbH TQSystems. *Servo-Kits ILM-70x18*. URL: https://www.tq-group.com/de/produkte/tq-robodrive/servo-kits-bremsen-sensoren/ilm70x18/ (visited on 08/01/2021) (cit. on p. 35).

[Vog47] A. Vogel. "Plan-Kerbverzahnungen". In: *Die Technik Berlin, Ost : techn.-wiss. Zeitschr. für Grundsatz- u. Querschnittsfragen* 2 (1947), pp. 89–92. ISSN: 0040-1099 (cit. on pp. 2, 6).

[Zha+14] Hailiang Zhang, Zhuoping Yu, Zaimin Zhong, Bonian Wu, and Xinbo Chen. "Modelica based modeling of automotive transmission". In: *2014 IEEE Conference and Expo Transportation Electrification Asia-Pacific (ITEC Asia-Pacific)*. IEEE. 2014, pp. 1–5 (cit. on p. 6).

## Selbstständigkeitserklärung

Hiermit versichere ich, Julia Richter, geboren am 28.05.1998 in Erfurt, dass ich die vorliegende Studienarbeit zum Thema

*Entwicklung und Aktuierung eines neuartigen Schaltgetriebes für die mobile Robotik*

ohne unzulässige Hilfe Dritter und ohne Benutzung anderer als der angegebenen Hilfsmittel angefertigt habe; die aus fremden Quellen direkt oder indirekt übernommenen Gedanken sind als solche kenntlich gemacht. Bei der Auswahl und Auswertung des Materials sowie bei der Herstellung des Manuskripts habe ich Unterstützungsleistungen von folgenden Personen erhalten:

*M. Sc. Alexander Kirst, Dipl.-Ing. Jens Reinecke*

Weitere Personen waren an der geistigen Herstellung der vorliegenden Studienarbeit nicht beteiligt. Mir ist bekannt, dass die Nichteinhaltung dieser Erklärung zum nachträglichen Entzug des Diplomabschlusses (Masterabschlusses) führen kann.

Dresden, den 31.08.2021 .....

Unterschrift